SPECTROSCOPY OF HIGH-SPIN STATES OF ^{206}Po

A.M. BAXTER

Department of Pysics and Theoretical Physics, Faculty of Science, Australian National University, Canberra ACT 2601 Australia

A.P. BYRNE, G.D. DRACOULIS, R.A. BARK, F. RIESS*, and A.E. STUCHBERY

Department of Nuclear Physics, Research School of Physical Sciences, ANU

and

M.C. KRUSE and A.R. POLETTI

Department of Physics, University of Auckland, Private Bag, Auckland, NZ

* Permanent address: Sektion Physik, LMU, Am Coulombwall 1, D8046, Garching, Germany

SPECTROSCOPY OF HIGH-SPIN STATES OF ^{206}Po

A. M. BAXTER

*Department of Physics and Theoretical Physics, Faculty of Science,
Australian National University, Canberra ACT 2601 Australia*

A. P. BYRNE, G. D. DRACOULIS, R. A. BARK, F. RIESS[1] and A. E. STUCHBERY

*Department of Nuclear Physics, Research School of Physical Sciences
Australian National University*
and
M. C. KRUSE and A. R. POLETTI

*Department of Physics, University of Auckland, Private Bag, Auckland,
New Zealand*

Abstract: The yrast and near-yrast energy levels of ^{206}Po have been investigated to over 9 MeV excitation and up to spins of $24\hbar$. The measurements consisted of $\gamma-\gamma$ coincidence data, internal-conversion-electron spectra, time spectra of γ-rays relative to a pulsed beam, excitation functions and γ-ray angular distributions. Two new isomers, with lifetimes in the one-nanosecond range, were found. The observed level structure is compared with the predictions of empirical shell-model calculations in which ^{206}Po is regarded as a ^{208}Pb core with two valence protons and four valence neutron holes. The agreement is generally satisfactory for the observed odd-parity levels and for even parity levels with $J > 12$; those with $J = 6$ to 12 are better accounted for by weak coupling of two valence protons to a ^{204}Pb core in its 0^+_1, 2^+_1 and 4^+_1 states.

E
NUCLEAR REACTIONS ^{198}Pt (^{13}C, 5n), $E = 70 - 80$ MeV; measured $\gamma\gamma(t)$, beam $\gamma(t)$, E_γ, I_γ, $I_\gamma(E)$, $I_\gamma(\theta)$, I_{ce}. ^{206}Po deduced levels, J, π, τ, $B(EL)$, ICC. Enriched targets, Ge, Si(Li) detectors, pulsed beam. Empirical shell-model calculations.

[1] Permanent address: Sektion Physik, LMU, Am Coulombwall 1, D8046, Garching, Germany

1. Introduction

Studies of the properties of the excited states of $^{210, 211, 212}$Rn [refs. [1-3])] have identified certain high-spin states (J>20), which are often isomeric, and which appear to involve the excitation of a neutron from the Z = 82, N = 126 core to one of the high-spin orbitals ($g_{9/2}$, $i_{11/2}$ or $j_{15/2}$) outside the N = 126 closed shell. Similar excited-core configurations have been assigned [4]) to high-spin isomers in $^{212, 213}$Fr. Despite the energy lost in promoting a neutron across the intershell gap, it is found [5]) that such states may compete successfully for positions in the yrast sequence because the interaction between an extra-core proton and an extra-core neutron, with both in high-spin orbitals, is strongly attractive [6]) when the two are aligned for maximum spin. In contrast, the interaction between an extra-core proton and a neutron hole, again both in high-spin orbitals and maximally aligned, is notably repulsive [6]).

It might be expected that the neutron-deficient isotopes of polonium (N < 126) would be as likely as those of radon to exhibit high-spin states involving the excitation of a neutron from the core. Evidence has been found [7]) for such a state in ^{209}Po. However, in previous work, no other Po isotope has been investigated to sufficiently high spin to observe excited-core states. The nucleus ^{206}Po, having two protons more and four neutrons less than ^{208}Pb, should be a good candidate for such studies as states with spins up to 30 ħ or greater are expected to be accessible by the ^{198}Pt(^{13}C,5n) reaction.

The yrast level scheme of ^{206}Po up to the 6$^+$ level has been well established [8]) by studies of ^{206}At electron-capture decay, ^{210}Rn α-decay and of levels populated in the (^{3}He,xn) and (^{4}He,xn) reactions. Prior to the present work, the most comprehensive information on the higher-spin states was that reported by Rahkonen et al. [9]); in that work levels up to 5.14 MeV excitation and having spins up to 16 ħ were identified. We present here a study of the yrast and near-yrast states of ^{206}Po which extends knowledge of the level scheme to 9 MeV excitation. Spins up to 24 ħ have been assigned and the results are compared with the predictions of shell-model calculations.

2. Experimental procedure

Excited states of ^{206}Po were populated with the ^{198}Pt (^{13}C, 5n) ^{206}Po reaction using the ^{13}C beam from the 14UD Pelletron accelerator at the Australian National University. The decay properties of the states were studied in several experiments the details of which are summarized in table 1. The targets consisted of self-supporting platinum foils, isotopically enriched to 95.8% in ^{198}Pt, fabricated by rolling the platinum metal. The foil thickness was 4.0 mg/cm^2 for all experiments except the internal conversion measurements for which it was 3.2 mg/cm^2.

All measurements were made at a bombarding energy of 78 MeV which was chosen as the optimum following measurements of the yield of γ-rays from ^{198}Pt (^{13}C, 5n) ^{206}Po, and from competing reactions (mainly the 6n channel), as a function of beam energy in the range 70 to 80 MeV. The energy loss of 78 MeV ^{13}C ions in a 4.0 mg/cm^2 target at 45° to the beam direction is about 5 MeV.

Two separate γ-γ coincidence experiments were conducted. In the first, time correlations in the range ± 2.5 μs were recorded between γ-rays detected in two Compton-suppressed spectrometers (CSS). Each CSS consisted of a hyperpure, coaxial, germanium (HPGe) detector of about 23% efficiency inside a NaI anti-Compton shield. Energy and efficiency calibrations were obtained using a ^{152}Eu source. In the second coincidence experiment four detectors were used: two large HPGe detectors (without Compton suppression) and two smaller, planar Ge detectors, (LEPS). This experiment was specifically intended for observation of cascades involving low-energy transitions ($E_\gamma \lesssim$ 60 keV), making use of the superior sensitivity, energy resolution and timing characteristics of the LEPS at such energies. Relative time differences in the range ± 0.5 μs were measured between the two HPGe detectors (summed) and the two LEPS (summed) and between the two LEPS.

To measure excited-state lifetimes in the range of about 0.2 to several hundred ns the ^{13}C beam was pulsed to give ~ 1 ns (FWHM) pulses separated by 1 μs. Time

spectra, relative to the beam pulses, were recorded of γ-rays detected in a large HPGe detector and also a LEPS. For determination of the longer lifetimes (~ 1 μs), these data were complemented by the γ-γ coincidence measurements.

Spectra of internal-conversion electrons emitted at 125° to the beam direction were obtained with a cooled Si(Li) detector and "mini-orange" magnetic filter [10]. This combination gave satisfactory electron-detection efficiency down to about 180 keV. The corresponding γ-ray spectrum was recorded simultaneously with a CSS at 55°. To aid in separating transitions above and below the longer-lived isomers, a pulsed beam was used, consisting of 1 ns (FWHM) pulses 1 μs apart. The data were sorted into spectra which were either prompt or delayed relative to the beam pulses.

Finally, angular distributions of γ-ray intensity were measured at eight angles in the range 45° to 155° with a rotatable HPGe detector. A similar detector, fixed at 90°, served as a monitor for normalisation.

3. Results

3.1 THE LEVEL SCHEME

The properties of the high-spin states of ^{206}Po, as determined in the present work, are summarized in fig. 1. In table 2, the observed γ-rays attributable to ^{206}Po are listed together with their locations in the level scheme, relative intensities and angular distribution coefficients. Two new isomers were found, however their lifetimes were ~ 1 nsec and they were of little help in deciding the ordering of transitions. Consequently, the level scheme above 2.5 MeV was deduced almost entirely from comparison of energy sums and from coincidence spectra obtained with the Compton-suppressed germanium detectors.

As mentioned earlier the yrast 0^+, 2^+, 4^+, 6^+ level sequence in ^{206}Po has been well-established by previous work. There is also evidence [9] that the yrast 8^+ level is just above the 6^+ level and that it is isomeric with a mean life of about 300 nsec.

It is therefore expected that the spectrum of γ-rays early with respect to the 395, 477 and 701 keV transitions (upper panel of fig. 2) will contain exclusively ^{206}Po γ-rays above the yrast 8$^+$ level (fig. 1) and give an indication of which are the most important decays. The main decay path from the 3462.8 keV level is by the 395.0 and 805.9 keV transitions (the order of which is uncertain) to the isomer at 2262.0 keV and thence via 61.8 and 614.6 keV transitions to the other previously-known isomer at 1585.6 keV. The spectrum in the lower panel of fig. 2, of early transitions minus late transitions relative to the 614.6 keV line, determines the ordering, with respect to these two longer-lived isomers, of a number of strong transitions and clearly demonstrates the existence of the doublet at 395 keV.

Although the transition immediately depopulating the 1585.6 keV level was not observed, it is assumed from the similarity of the ^{206}Po decay scheme in this region to those of ^{208}Po [ref. [11])] and ^{210}Po [ref. [12])], and from the g-factor measurements of Bräuer et al. [13]), that this is the 8$^+$ state arising from the $\pi(h_{9/2}^2)$ configuration. Its excitation energy is inferred from observation of a weak 627.1 keV line which is in prompt coincidence with the 61.8, 395.5, 477.0 and 700.6 keV γ-rays, but not with the 614.6 keV transition. Thus the 8$^+$ level is at 1585.6 keV and it decays to the 6$^+$ level by an unobserved, 12.5 ± 0.1 keV, E2 transition.

The 3462.8 keV level also decays by two subsidiary paths: one via the 806.6, 237.6 and 833.0 keV transitions and the other through the 252.5, 429.3, 167.9, 189.8, 837.2 and 1027.3 keV cascade. The 3462.8 keV level is populated almost exclusively by the 86.0 keV transition and, above about 3.5 MeV, the decay scheme separates rather cleanly into two sets of levels according to their parities. The spectra in fig. 3 illustrate the principal decay paths between the 5935.0 and 3462.8 keV levels. These spectra are of γ-rays in prompt coincidence (± 140 nsec) with certain key transitions; this rather wide time range was chosen to allow for the time walk arising from the slower risetimes of low-amplitude pulses from the large, coaxial, Ge detectors.

The main decay path from the 5935.0 keV level through the odd-parity levels is via the 557.7, 744.8, 469.6 and 595.8 keV transitions. The top panel of fig. 3 shows

the spectrum of γ-rays in coincidence with the 595.8 keV transition and the 557.7, 744.8 and 469.6 keV lines are prominent. The ordering of these four transitions is established unambiguously by several cross-over transitions and by the excitation functions shown in fig. 4.

The decay of the 5935.0 keV level through the group of even-parity levels is more complex. Energy sums and γ-γ coincidence data demand that the 1103.3, 722.4, 380.6, 146.2, 600.8, 179.5 and 682.0 keV transitions be placed as shown in fig. 1 and the spectrum of γ-rays in coincidence with the 146.2 keV line (fig. 3) illustrates these relationships.

The 600.8, 165.6, 457.0 keV cascade connects the 5935.0 keV level to another at 4711.6 keV which then decays either by a strong 1144.5 keV transition, which is in coincidence with the 86.0, 806.6, 237.6 keV cascade (see fig. 3), or by the weaker 481.3, 526.2, 1285.6 keV sequence. Both these paths terminate at the 2418.6 keV level and comparison of the energy sums involved shows a difference of 18.4 keV. This discrepancy and other coincidence data require an unobserved 18.3 keV transition between the 1144.5 and 86.0 keV decays. The 3567.1 keV level, which is de-excited by the 18.3 keV transition, is also fed by the strong 557.7, 744.8, 469.6, 595.8 keV cascade.

The 146.2 keV line is in prompt coincidence with most of the γ-rays lying below it in the scheme (fig. 3) and about 30% of the decay strength from the 4685.6 keV level is through the 1064.1 keV transition. The 146.2 and 1064.1 keV decays are linked by the 33.7 and 39.0 keV lines. These low-energy γ-rays could be seen in certain of the spectra projected from the array of coincidence events between the HPGe and LEPS detectors; examples of these spectra are shown in fig. 5. In the top panel is the LEPS spectrum in coincidence with the 380.6 keV line in the HPGe detectors. Peaks at 33.7 and 39.0 keV can be seen clearly and, although they appear to be weak, the transitions can carry the decay intensity required of them provided they have predominantly M1 multipolarity. A peak at 44.0 keV can also be seen in this spectrum and this transition, in cascade with those at 33.7 and 39.0 keV, makes the connection between the 4685.6 and 4568.8 keV levels

required by the coincidence data. In the lower panel of fig. 5 is the γ-ray spectrum in coincidence with the 39.0 keV line in the LEPS; the 146.2, 380.6 and 1064.1 keV γ-rays are among the more prominent, consistent with the placement of the 39.0 keV transition. The spectrum in coincidence with the 33.7 keV line in the LEPS was qualitatively similar although considerable weaker. The ordering of the 146.2, 33.7, 39.0 and 1064.1 keV decays is established by several parallel transitions. The energies and placements of the 39.0, 1064.1, 1045.9 and 1084.8 keV γ-rays provide further evidence for the existence of the unobserved 18.3 keV transition which depopulates the 3567.1 keV level.

Above 5.9 MeV excitation the principal feature of the decay scheme is the cascade of three strong transitions (183.2, 169.8 and 467.7 keV) populating the 5935.0 keV level. Above these three transitions, the feeding strength appears to be shared by a fairly large number of relatively weak transitions as can be seen (fig. 6) in the spectrum in prompt coincidence with the 183.2 keV γ-rays.

Prominent lines at 212.4 and 350.8 keV appear in the spectra in coincidence with essentially every ^{206}Po γ-ray except those in the cascades populating the 5874.2 and 6009.5 keV levels. Coincidence spectra obtained with gates on the 212.4 and 350.8 keV lines are closely similar except that each sees the other strongly. (See for example the 212 keV coincidence projection in fig. 6.) The coincidence relationships indicate that these two transitions are located together at high excitation which is consistent with the evidence (fig. 4) of the excitation functions.

The 350.8 and 212.4 keV transition appear to populate a level at 8430.6 keV immediately below which the decay strength is fragmented over a number of relatively weak paths most of which then merge again to populate the 5935.0 keV level. The ordering of transitions in the 957.3, 336.7, 793.6, 292.9, 115.5 keV cascade is determined partly by their relative intensities and also by the observations that the higher members of the cascade have coincidence links with the 169.8 and 183.2 keV γ-rays whereas the lower members do not. Explicit decay paths linking this cascade with the 6288.0 and 6118.2 keV levels could not however be found.

The spectra in coincidence with the 212 and 351 keV gates indicate that the 8430.6 keV level also has significant decay paths which include 581.1, 662.1 and 936.5 keV γ-rays. In all-three cases, these energies correspond closely to unresolved doublets which have been placed elsewhere in the scheme, however it was not possible to establish the decay sequences from the 8430.6 keV level involving these γ-rays. The HPGe - LEPS coincidence data show that a 43.1 keV γ-ray is closely associated with 212.4 and 350.8 keV lines and, although it is likely that this low-energy transition also plays a significant part in the decay of the 8430.6 keV level, it too could not be placed in the decay scheme.

3.2 EXCITED STATE LIFETIMES

Two isomers in ^{206}Po, the 8^+ level at 1535.6 keV and the 9^- level at 2262.0 keV had been established [9] prior to the present work. Even though knowledge of the level scheme has been greatly extended by the experiments reported here, only two additional isomers were found, both with comparatively short mean lives (<2 ns).

New values for the lifetimes of the 8^+ and 9^- isomers were extracted from the γ-γ coincidence data; these data were obtained with a time range ($\pm$ 2.5 μs) better suited to measurements of longer lifetimes than that (1 μs) used in the pulsed-beam experiment. Representative time spectra used for this purpose are shown in fig. 7. The upper panel of fig. 7 shows the time spectrum of 477.0 keV γ-rays relative to the 614.6 keV transition and illustrates the effect of the 8^+ isomer at 1585.6 keV. The spectrum in the lower panel demonstrates that one member of the 395.0/395.5 keV doublet lies above the 614.6 keV transition, the other is below and an isomer intervenes in each case. The values obtained for the mean lives of the 8^+ and 9^- isomers are given in table 3; each is the weighted mean of four essentially independent determinations. The results of previous measurements are also given.

For the measurement of lifetimes in the nanosecond range the time of detection of γ-rays relative to 1 ns-wide beam pulses was recorded in spectra with

a dispersion of 0.2 ns/channel. Time spectra for γ-rays known to be prompt relative to the arrival of the beam pulse (i.e., intervening lifetimes < 0.1 ns) were fitted with a skewed Gaussian function. Such "prompt" lines were provided by γ-decays following ^{198}Pt + ^{13}C inelastic scattering and from the ^{208}Pb(^{13}C, 3n) ^{218}Ra reaction which was run, immediately following the ^{198}Pt + ^{13}C experiment, with identical pulsed-beam conditions and electronics arrangement. The dependences on γ-ray energy of the parameters of the skewed Gaussian were fitted with suitable polynomial functions and the coefficients of these polynomials then specified a so-called prompt response function (PRF). The time spectra of ^{206}Po γ-rays were fitted with a convolution of the PRF appropriate to the energy of the γ-ray and an exponential function representing the lifetime of the emitting state. If the γ-rays in question did not directly depopulate the isomer, a PRF contribution could be added to take account of side-feeding. Apart from those transitions whose time spectra were influenced by the known 8^+ and 9^- isomers, only two transitions (the 212.4 and 237.6 keV lines), definitely attributable to ^{206}Po, showed time spectra which differed significantly from the PRF.

For the 237.6 keV transition de-exciting the 2656.2 keV level, the time spectrum is shown in fig. 8 and the mean life involved was found, from the fitting procedure described above, to be 0.7 ± 0.2 ns. This lifetime was assigned to the 11^- state at 2656.2 keV since none of the transitions feeding this state showed any significant deviation from prompt behaviour.

For the 212.4 keV line a mean life of 1.5 ± 0.4 ns was obtained. The 350.8 keV transition did not show this lifetime; this implies the ordering of these transitions shown in fig. 1 and that the lifetime can be assigned to the level directly depopulated by the 212.4 keV γ-rays.

3.3 SPIN AND PARITY ASSIGNMENTS

The spin and parities of the levels shown in fig. 1 were, in most cases, deduced from measurements of internal-conversion coefficients and γ-ray angular distributions. In addition. for a number of the low-energy transitions

($\leq$ 260 keV), values of total internal-conversion coefficients were inferred from balancing the intensities of transitions feeding a level with those depopulating it. The conversion-electron data are shown in fig. 9; one pair of spectra (electrons and γ-rays) contains transitions which occurred within the range +20 to -40 ns relative to the 1 ns-wide beam pulse while the other contains those which were delayed by 40 to 900 ns with respect to the beam pulse. The internal-conversion coefficients which were calculated from these spectra and those calculated from intensity balances are listed in table 4 together with the multipolarities deduced from comparison with the calculation of Rösel et al. [14]).

The γ-ray angular distributions were fitted with the usual expansion in even-order Legendre polynomials; the coefficients are listed in table 2. These data also provided the basis for most of the determinations of γ-ray relative intensities.

As discussed earlier it is assumed, on the basis of comparison with the [208, 210]Po level schemes, that the 1585.6 keV level is the yrast 8+ state. The 2422.8, 2612.7, 2780.6, 2901.4, 3209.9 and 3462.8 keV levels are then assigned J^{π} values of 9+, 10+, 11+, 12+, 12+ and 13- respectively by the stretched transitions of known multipolarity connecting them.

In the main cascade, the 805.9 keV line is a stretched E2 transition and internal-conversion measurements indicate predominant E2 multipolarity for the 395.0 keV transition. The angular distribution of the latter γ-ray is obscured by that of the stronger 395.5 keV line. The angular distributions of the 614.6 and 61.8 keV lines are attenuated by relaxation during the lifetime of the 2262.0 keV level, however the internal-conversion measurements indicate M1 for the 614.6 keV transition and the 61.8 keV line is assigned E1 from consideration of intensity balance. Given that J^{π} (3462.8 keV) = 13-, these results, together with the observation of the 627.1 keV line, yield J^{π} = 8+ and 9- for the 2200.2 and 2262.0 keV levels respectively. The indication from the K-shell conversion data (table 4) that the 676.4 keV transition is E2 must therefore be incorrect. Presumably the K-shell conversion line is contaminated and the L-shell coefficient, which favours E1, is the more reliable. The 2418.6 and 2656.2 keV levels are assigned 10+ and 11-

respectively from the observed multipolarites of the 806.6, 237.6 and 833.0 keV transitions.

The 86.0 keV transition is found to be a stretched M1 from its angular distribution and from intensity balance for the 3462.8 keV level. The 3548.8 level is therefore assigned $J^\pi = 14^-$. The multipolarity of the unobserved 18.3 keV transition can be inferred by the following reasoning. If the 3567.1 keV level had a lifetime longer than 0.5 ns, the effect of this lifetime would be obvious in the time spectra, relative to the beam pulses. of the 805.9 and 806.6 keV γ-rays. A lifetime shorter than 0.5 ns implies that, if the 18.3 keV transition were pure E2, it would have a strength greater than 400 Weisskopf units (W.u.). Although perhaps not impossible, this strength would be extraordinarily large for a transition such as this and we therefore conclude that it is predominantly dipole. A loop of transitions of well-established multipolarities, viz., 595.8 keV (M1), 469.5 (M1), 744.8 (M1), 557.7 (M1), 1103.3 (E1), 146.2 (M1), 33.7 (M1), 39.0 (M1) and 1064.1 (E1), linking the 3567.1 and 3548.8 keV levels requires that there be no parity change in the direct transition between them. The 18.3 keV transition must therefore be predominantly M1. We assume that it is a stretched M1, giving $J^\pi(3567.1) = 15^-$, as one would expect this level, which plays such a pivotal role in the decay scheme, to be an yrast state. The cascade of stretched M1 transitions feeding the 3567.1 keV level then leads to assignments of 16^-, 17^-, 18^- and 19^- respectively to the levels at 4162.9, 4632.5, 5377.3 and 5935.0 keV.

The spin and parity assignments to the 4685.6 (17^+), 4831.8 (18^+) and 5212.4 keV (19^+) levels depend upon the 19^- assignment to the 5935.0 keV level and the multipolarities of the 1103.3, 146.2 and 380.6 keV γ-rays. The angular-distribution data indicate that all three are stretched transitions. Other assignments to the even-parity levels in the region come from the 1064.1 keV, stretched E1 transition, the M1 multipolarity of the 33.7, 39.0 and 44.0 keV γ-rays and from the 179.5 (M1), 165.6 (M1), 457.0 (M1) and 1144.5 keV (E1) cascade of stretched dipole transitions.

The three stretched M1 transitions (183.2, 169.8 and 467.7 keV) give assignments of 20^-, 21^- and 22^- to the 6118.2, 6288.0 and 6755.7 keV levels

respectively. The angular-distribution data have yielded spins for some of the higher-excitation levels but their decays were not sufficiently strong for internal-conversion measurements.

To summarize, the present work has established the high-spin states of ^{206}Po, and their principal decay modes, up to the 22$^-$ level at 6755.7 keV in the case of odd-parity states and to the 19$^+$ level at 5513.7 keV for the even-parity states. Above about 6.5 MeV excitation, the decay strength is apparently shared between a large number of paths; owing to the weakness of most of them, it has been possible to assign spins only to a few of the levels concerned.

4. Discussion

4.1 EMPIRICAL SHELL-MODEL CALCULATIONS

The excitation energies of the yrast and near-yrast levels of ^{206}Po were calculated using the semi-empirical shell model developed for the lead region by Blomqvist and co-workers [15]. In this approach pure configuations are assumed, and, as far as possible, experimentally-determined values are used for both single-particle energies and two-nucleon interaction energies. Two sets of calculations were carried out: in one the ^{206}Po nucleus was regarded as an inert ^{208}Pb core with two valence protons and four valence neutron holes, while in the other we calculated either the energies of two valence protons coupled to a ^{204}Pb core or of four valence neutron holes coupled to a ^{210}Po core.

4.1.1 Calculations with a ^{208}Pb core. In the first set of calculations the excitation energy E_x of the state in a specified configuration is given by

$$E_x = E_{SP} - E_{GS} + E_{INT}$$

where E_{SP} is the sum of the empirical single-particle energies, relative to the ^{208}Pb core, obtained from ^{209}Bi for protons and ^{207}Pb for neutron holes, E_{GS} is the energy of the ^{206}Po ground state relative to the ^{208}Pb core [21273 ± 11 keV, ref. [16])]

and E_{INT} is the combined effect of all the interactions between the valence particles and holes. It was assumed that only two-nucleon interactions would contribute significantly to E_{INT}; empirical values of the interaction energies were obtained from the tabulations of Lönnroth [6] with a few corrections to take account of more recent experimental data [17]. Where experimental values were not available, the theoretical values of Kuo and Herling [18] were used or, in a few cases where even such calculations were absent, reasonable estimates were made. The values of E_{INT} for a particular spin in a given configuration were obtained by diagonalizing the matrix of interaction energies corresponding to all possible couplings giving that spin.

The configurations which might be expected to contribute to the yrast or near-yrast states of ^{206}Po are listed in table 5 together with their values of $E_0 = E_{SP} - E_{GS}$ which is the excitation energy of a configuration unperturbed by the two-nucleon interactions. The calculated excitation energies of the higher-spin states in each configuration are summarized and compared with the observed levels in figs. 10 and 11; for each configuration only the lowest energy state for a given spin is included. For some configurations the calculations involved a substantial number of two-nucleon interaction energies not derived from experimental data; i.e., they were estimated or taken from the calculations of Kuo and Herling [18]. In these cases, which are identified in figs. 10 and 11, the level energies will be subject to an additional uncertainty, possibly of several hundred keV, apart from that arising from any inadequacy in the shell-model description of ^{206}Po. For the sake of clarity in the following discussion even-parity and odd-parity states are, for the most part, considered separately.

Even-parity levels have been established experimentally up to the $J = 19$ level at 5514 keV and, according to the calculations, the yrast states with $J \leq 20$ should be almost entirely confined to the $\pi(h_{9/2}^2) \, \nu(p_{1/2}^{-2}f_{5/2}^{-2})$ and $\pi(h_{9/2}i_{13/2})$ $\nu(p_{1/2}^{-2}f_{5/2}^{-1}i_{13/2}^{-1})$ configurations. Up to 3 MeV excitation the observed levels are not well described (fig. 10) by the calculations. Although the energies of the 0^+, 6^+ and 8^+ states of the $\pi(h_{9/2}^2) \, \nu(p_{1/2}^{-2}f_{5/2}^{-2})$ configuration agree reasonably well with

those observed for the ground state, the 6$^+$ level and the 8$^+$ level at 1586 keV, the energies of the 4$^+$, 9$^+$, 10$^+$, 11$^+$ and 12$^+$ states of this configuration are all much too low compared with their likely experimental counterparts. Indeed, the 4$^+$ state is predicted to fall below the first 2$^+$ state. This low-lying 4$^+$ state comes mostly from the $\nu(f_{5/2}^{-2})_{4^+}$ coupling; it appears (see subsect. 4.1.3) that the calculations do not treat the interactions of the four neutron holes adequately and that the 4$^+$ level observed at 1178 keV probably owes more to the $\pi(h_{9/2}^2)_{4^+}$ coupling than to the neutron holes. The observed even-parity levels with $J = 6$ to 12 are considerably better accounted for by the simpler calculations, described later (subsect. 4.1.3), which involve two valence protons and a ^{204}Pb core.

Above 3 MeV the observed energies of the even-parity states are fairly well reproduced by the calculations and it is noticeable (fig. 1) that the bunching of the $J^\pi = 14^+$ to 18^+ levels near 4.6 MeV has a counterpart in the closely-spaced group of states near 4.45 MeV of the $\pi(h_{9/2}i_{13/2})\,\nu(p_{1/2}^{-2}f_{5/2}^{-1}i_{13/2}^{-1})$ configuration. This bunching gives rise to the observed low-energy transitions between the 4686 (17$^+$), 4652 (16$^+$), 4613 (15$^+$), 4569 (14$^+$) and 4483 keV levels. The high-energy transitions from the 4569 and 4483 keV levels to those at 2781 (11$^+$), 2901 (12$^+$) and 3201 keV (12$^+$) presumably reflect the large energy gap between the $\pi(h_{9/2}i_{13/2})\,\nu(p_{1/2}^{-2}f_{5/2}^{-1}i_{13/2}^{-1})$ and $\pi(h_{9/2}^{-2})\,\nu(p_{1/2}^{-2}f_{5/2}^{-2})$ configurations. Apart from the group of levels near 4.6 MeV, it is not possible, in the absence of experimental evidence other than level energies and decay modes, to attribute other even-parity levels in this excitation region to any particular configuration. For example, on the available evidence, any of three configurations could account for the 19$^+$ level at 5514 keV.

Similarly, for even-parity levels with $19 < J \leq 24$, a number of configurations could contribute to the yrast level scheme. However, for $J > 24$, it is necessary to invoke the $i_{13/2}^{-3}$ coupling for neutron holes and $h_{9/2}i_{13/2}$ for protons. For example the $\pi(h_{9/2}i_{13/2})\,\nu(p_{1/2}^{-1}i_{13/2}^{-3})$ and $\pi(h_{9/2}i_{13/2})\,\nu(f_{5/2}^{-1}i_{13/2}^{-3})$ configurations can produce states with J^π up to 28$^+$ and 30$^+$ respectively. However, owing to the strong repulsion [889 keV, ref. [6]] between the $h_{9/2}$ proton and $i_{13/2}$ neutron hole when

aligned for maximum spin, the highest-spin states of these configurations are predicted to occur above 10 MeV and it is likely that, at this energy, core excitation will have become significant.

The lowest-lying, odd-parity level observed in the present work is the isomeric 9^- level at 2262 keV. There can be little doubt that it belongs to the $\pi(h_{9/2}^2)$ $\nu(p_{1/2}^{-2}f_{5/2}^{-1}i_{13/2}^{-1})$ configuration and is analogous to the 9^- isomer in ^{204}Pb. The same configuration probably accounts for most of the observed odd-parity levels (see fig. 11) up to the 17^- level at 4633 keV with the $\pi(h_{9/2}\,i_{13/2})\,\nu(p_{1/2}^{-2}f_{5/2}^{-2})$ configuration playing a subsidiary role. In particular the closely-spaced 13^-, 14^- and 15^- levels observed at 3463, 3549 and 3567 keV can be identified with the similar group in the $\pi(h_{9/2}^2)\,\nu(p_{1/2}^{-2}f_{5/2}^{-1}i_{13/2}^{-1})$ configuration although the latter are about 200 keV too low.

It seems reasonable to identify the observed 19^-, 20^- and 21^- levels at 5935, 6118 and 6288 keV respectively with the states of corresponding spin and parity in the $\pi(h_{9/2}i_{13/2})\,\nu(p_{1/2}^{-2}i_{13/2}^{-2})$ configuration. The energies match well and the nearest 21^- state in any other configuration is calculated to be at 7296 keV, over 1 MeV too high. These three levels are linked by the very prominent 169.8 and 183.2 keV transitions. The 18^- and 17^- states of the $\pi(h_{9/2}i_{13/2})\,\nu(p_{1/2}^{-2}i_{13/2}^{-2})$ configuration fall within 50 keV of the 19^- state which would inhibit decay of the latter to either of the former two. The observation then that the 19^- level at 5935 keV has four competing decay routes of comparable intensity is consistent with identifying it with the 19^- state of the $\pi(h_{9/2}i_{13/2})\,\nu(p_{1/2}^{-2}i_{13/2}^{-2})$ configuration as proposed above. Assuming this identification is correct the 722.4 and 1103.3 keV transitions would then be to the 19^+ and 18^+ states of the $\pi(h_{9/2}i_{13/2})\,\nu(p_{1/2}^{-2}f_{5/2}^{-1}i_{13/2}^{-1})$ configuration, the 600.8 keV transition would be to the 18^+ state of the $\pi\,(h_{9/2}i_{13/2})\,\nu(p_{1/2}^{-1}f_{5/2}^{-2}i_{13/2}^{-1})$ configuration and the 557.7 keV transition would have to be to the 18^- state of the $\pi(h_{9/2}^2)\,\nu(p_{1/2}^{-1}f_{5/2}^{-2}i_{13/2}^{-1})$ configuration.

The highest-spin, odd-parity, yrast state which can be produced by the configurations listed in table 5 is $J^\pi = 27^-$ from the $\pi(h_{9/2}i_{13/2})\,\nu(f_{5/2}^{-2}i_{13/2}^{-2})$ configuration. It is calculated to occur at 9417 keV and may correspond to the

observed level at 8994 keV.

4.1.2 Excited-core states. It is of interest to estimate the energy at which states involving core excitation might first appear in the yrast sequence. Two examples are given: for even-parity states the configuration is $\pi(h_{9/2}^2)$ $\nu(p_{1/2}^{-2}f_{5/2}^{-2}i_{13/2}^{-1}g_{9/2})$, giving spins up to 23ħ, while for odd-parity states it is $\pi(h_{9/2}i_{13/2})$ $\nu(p_{1/2}^{-2}f_{5/2}^{-2}i_{13/2}^{-1}g_{9/2})$, giving spins up to 26ħ.

Roy et al.[19] have observed four 10^+ states in ^{208}Pb, populated by the ^{209}Bi(t, α) reaction, at excitations ranging from 4.89 to 5.93 MeV. They identified these states with 1p - 1h excitations and found that the lowest three have significant $\nu(i_{13/2}^{-1}g_{9/2})$ components in their wave functions. The mean of the excitation energies of the 10^+ states weighted by the square of the amplitudes of these components is 5.04 MeV. The maximum spin which may be obtained from the $\nu(i_{13/2}^{-1}g_{9/2})$ configuration is 11^+ and there is some evidence, from (e, e') work [17], for an 11^+ level at 5.27 MeV in ^{208}Pb. However, as the core-excited states with spin $J_{max}-1$ are expected to be favoured over those with J_{max}, it is the former which are considered here.

The excitation energies of the core-excited states are estimated, assuming weak coupling, by adding the calculated energy (5.04 MeV) of the $\nu(i_{13/2}^{-1}g_{9/2})_{10+}$ excitation to the energy in ^{206}Po of the parent, valence configurations. Under this assumption the interactions of the $g_{9/2}$ neutron and $i_{13/2}$ neutron hole with the valence protons and neutron holes are neglected. Although in individual cases these two-nucleon interactions may be several hundred keV, the attractive proton-neutron interactions tend to cancel the repulsive proton-neutron hole energies such that the total of the two-body interactions of the $g_{9/2}$ neutron and $i_{13/2}$ neutron hole is not expected to exceed 500 keV.

In the even-parity example, the parent state is taken as the observed 12^+ level at 2901 keV which should have a strong $\pi(h_{9/2}^2) \nu(p_{1/2}^{-2}f_{5/2}^{-2})$ component. With the $\nu(i_{13/2}^{-1}g_{9/2})$ excitation a $J^\pi = 22^+$ excited-core state would be expected at $2900 + 5040 = 7940$ keV. This is about 1 MeV above the observed yrast line. For the odd-parity case the particle-hole excitation is added to the excitation energy (3670

keV) calculated for the 15$^-$ level of the $\pi(h_{9/2}i_{13/2})$ $\nu(p_{1/2}^{-2}f_{5/2}^{-2})$ configuration to give a 25$^-$ state at 8710 keV. Now, although it was not possible to assign $J^\pi = 25^-$ to any of the levels observed in the present work, the 8430.6 keV level is connected by three, parallel, two-step cascades to lower levels having $J = 23$. The 8430.6 keV level is therefore likely to have $J = 25$ or 26. It is populated by the prominent 212.4 keV transition but decays by a number of weak transitions indicating that its structure is substantially different from that of the levels below it. Thus, bearing in mind the uncertainties involved in the weak-coupling calculation, the 8430.6 keV level appears to be a good candidate for an excited-core state, most likely the $J = 25$ member of the $\pi(h_{9/2}i_{13/2})$ $\nu(p_{1/2}^{-2}f_{5/2}^{-2}i_{13/2}^{-1}g_{9/2})$ configuration.

4.1.3 Calculations with a ^{204}Pb core or a ^{210}Po core The observed level scheme of ^{206}Po is reasonably well accounted for overall by the shell-model calculations described in subsect. 4.1.1. However the agreement is not good for most levels with $J \leq 12$ and it is believed that the discrepancies are caused mostly by the use of empirical two-neutron-hole interaction energies from ^{206}Pb. The levels of ^{206}Pb with $J \leq 4$ have highly-mixed configurations drawn from the $p_{1/2}$, $f_{5/2}$ and $p_{3/2}$ orbitals. This mixing will be partially blocked in ^{206}Po by the two additional neutron holes and, consequently, the ^{206}Po levels with low-spin, neutron-hole configurations will not be as low in energy as the empirical interactions from ^{206}Pb indicate they should be. This proposition is supported by the fact that calculations of the kind described in subsect. 4.1.1 reproduce very well the energies of the high-spin levels of ^{204}Pb and ^{205}Pb but do not give a good account of the lower-spin yrast levels of these nuclei. For the levels of ^{206}Po with $J = 6$ to 12 we therefore carried out some calculations in which two valence protons in the $h_{9/2}$, $f_{7/2}$ and $i_{13/2}$ orbitals are coupled to a ^{204}Pb core in its ground and first 2$^+$ and 4$^+$ states. The single-particle energies were obtained from ^{205}Bi, adopting the identifications by Lönnroth [20] and Hübel et al. [21] of certain observed ^{205}Bi levels with single proton states relative to a ^{204}Pb(0$^+$) core, and with the multiplets formed by weak coupling of an $h_{9/2}$ proton to ^{204}Pb(2$^+_1$) and ^{204}Pb(4$^+_1$) cores. It should be noted that, in the $\pi(h_{9/2}) \otimes {}^{204}$Pb (4$^+_1$) coupling, the identifications are

less well established than in the other cases. The single-particle data required
for the present calculations are summarized in table 6.

The empirical interaction energies for the two protons were taken from the
appropriate levels of ^{210}Po. However there is experimental evidence [e.g., refs [22],
[23])] that these energies should be modified because the core is ^{204}Pb, not ^{208}Pb.
This so-called core-polarization interaction arises from virtual excitation of the
core by one proton and de-excitation by the other. Blomqvist et al. [22]) represent the
interaction with a quadrupole - quadrupole coupling which, for two extra-core
protons with spins j_1 and j_2 coupled to a resultant spin J, gives [24]) an interaction
energy

$$\Delta_{pol} = \chi \left\{ \frac{3}{32} \frac{X(X+1)}{j_1(j_1+1)j_2(j_2+1)} - \frac{1}{8} \right\}$$

where $X = J(J+1) - j_1(j_1+1) - j_2(j_2+1)$ and χ is a coupling parameter which
reflects the softness of the core. For a ^{208}Pb core $\chi = 0$, while for a ^{20}-Pb core
Blomqvist et al. [22]) find that $\chi = -1100$ keV gives a good account of the differences
between observed and calculated energies of the 6^+_1, 8^+_1 and 11^-_1 levels of ^{206}Po.
We also have used $\chi = -1100$ keV and, in the absence of any evidence to the
contrary, we assumed that the core-polarization correction for ^{204}Pb in its lowest
2^+ and 4^+ states is the same as that for the ground state; that is, it is given by the
above expression for Δ_{pol} with $\chi = -1100$ keV.

The results of these calculations are summarized in fig. 12 and compared
with the corresponding part of the observed level scheme. It should be noted that
for the 6^+, 8^+_1, 8^+_2 and 11^-_1 levels, these calculations are essentially the same as
those carried out by Rahkonen et al. [9]); the only difference is that they used $\chi = -1000$ keV instead of -1100 keV. It can be seen (fig. 12) that good agreement is
obtained between the excitation energies calculated for these simple
configurations and those of their likely experimental counterparts. Furthermore
the agreement is significantly improved by the inclusion of the core-polarization

correction, not only for the 6^+, 8^+_1 and 11^-_1 levels where this is to be expected since they were used in deducing the value $\chi = -1100$ keV, but for all but one of the other six levels as well. The mean of the magnitudes of the differences between calculated and observed energies for these six cases was reduced from 52 to $\overline{38}$ keV by inclusion of the core-polarization correction.

The good agreement between experimental excitation energies and those calculated for the simple configurations involving a ^{204}Pb core contrasts with the relatively poor account (figs. 10 and 11) of these levels provided by the more sophisticated calculations involving a ^{208}Pb core and six valence nucleons. This is consistent with the conclusion that, when the four neutron holes are coupled to low spin ($J = 0$ to 4), the two-neutron-hole interaction energies from ^{206}Pb levels may not be appropriate owing to the strong configuration mixing in the latter cases.

Also included in fig. 12 is the result of a simple shell-model calculation of the excitation energy of the 9^- state arising from the $\pi(h_{9/2}^2)_{0+}\, \nu(p_{1/2}^{-2}f_{5/2}^{-1}i_{13/2}^{-1})$ configuration in which the interaction energy between the valence nucleons is not completely reduced to a combination of two-nucleon interactions. As in the first set of calculations (subsect. 4.1.1) the excitation energy E_x of the configuration may be expressed as

$$E_x = E_{SP} - E_{GS} + E_{INT}$$

where E_{SP} is the sum of the single-particle energies relative to a ^{208}Pb core and E_{GS} is the ^{206}Po ground-state energy relative to that core. However in the present case the total interaction energy E_{INT} was calculated from empirical values for the $(h_{9/2}^2)_0$ and $p_{1/2}^{-2}$, two-nucleon interaction energies and from empirical interaction energies for all pair-wise combinations, with appropriate spins, of these two and the $f_{5/2}^{-1}$ and $i_{13/2}^{-1}$ neutron holes. These interaction energies were obtained from experimental data for ^{205}Pb [refs. [16, 25)]], ^{206}Pb [refs. [16,26)]],

[208]Po [ref. [16])] [209]Po [refs. [16,27])] and [210]Po [ref. [16)]. The calculation gives $E_x = 2271$ keV for the 9^- state of the $\pi(h_{9/2}^2)_{0+} \, \nu(p_{1/2}^{-2} f_{5/2}^{-1} i_{13/2}^{-1})$ configuration. No correction for core polarization has been made because, with the two protons coupled to zero resultant angular momentum, the ground-state configuration of [210]Po is probably mixed, and it would therefore be misleading to use $j_1 = j_2 = 9/2$ in the calculation of Δ_{pol}. This calculated excitation energy agrees very much better with the experimental value for the yrast 9^- level (2262.0 keV) than does that (1926 keV) for the lowest 9^- state of the $\pi(h_{9/2}^2) \, \nu(p_{1/2}^{-2} f_{5/2}^{-1} i_{13/2}^{-1})$ configuration obtained in the first set of calculations which involved a complete reduction to two-nucleon interactions and in which the resultant spin of the valence protons was not restricted to zero. This is probably due to the fact that, in the simpler calculation, the use of interaction energies from configurations similar to those in [206]Po means that the calculation includes, to some extent, the configuration mixing which no doubt arises when the spins of the valence nucleons are not coupled to produce the maximum resultant.

4.2 TRANSITION PROBABILITIES

Reduced transition probabilities calculated from the lifetimes measured in the present work are given in table 7; two are new results and the other two confirm values from earlier work [9]). With the measurement of the $8^+_1 \rightarrow 6^+_1$ transition energy, it is now possible to calculate unambiguously the reduced probability, B(E2) for this transition. The value of 2.35(4) W.u. is consistent with the trend in the neighbouring even-mass polonium isotopes; these are 1.11(16) W.u. for [210]Po [refs.[12,28])], 1.60(10) W.u. for [208]Po [refs.[11,28])] and 3.52(5) W.u. for [204]Po [refs.[29,30])]. The steady increase as N decreases below the N = 126 closed shell presumably reflects increasing admixtures of 2^+ collective components in the states concerned. This is supported by the close agreement between the ratio of the B(E2;$8^+_1 \rightarrow 6^+_1$) values for [206]Po and [208]Po (ratio = 1.45 ± 0.09) with the ratio of the quadrupole polarizabilities, defined [22]) as B(E2;$0^+_1 \rightarrow 2^+_1$) / $E_x(2^+_1)$, for the corresponding [204]Pb and [206]Pb cores (ratio = 1.44 ± 0.02).

The $9^-_1 \to 8^+_1$, transition (table 7) is strongly hindered and, as has been remarked elsewhere [9]), this suggests rather pure $\nu(j^{-2}_0\, f_{5/2}^{-1} i_{13/2}^{-1})$ and $\pi(h^2_{9/2})$ configurations for the 9^-_1 and 8^+_1 states respectively. The lifetime obtained in the present work of 0.7(2) ns for the 2656.2 keV level gives a hindrance of 4×10^4 for the $11^-_1 \to 10^+_1$, E1 transition. This is intermediate between the values 2.2×10^5 for ^{208}Po [refs. [31,32]] and about 2×10^4 for ^{204}Po. Using the lifetime and transition energy given by Rahkonen and Lönnroth [29]), we calculated the hindrance for ^{204}Po to be 2.3×10^4 or 1.7×10^4 depending on whether the transition energy of 93.1 keV is respectively greater or less than the K-shell binding energy of 93.105 keV in polonium. We conclude therefore that the small value of 1.4×10^3 given and remarked upon by Rahkonen and Lönnroth is incorrect.

5. Summary and conclusions

In the work reported here we have extended knowledge of the yrast and near-yrast states of ^{206}Po up to about 9 MeV excitation. Two new isomers, with lifetimes in the one-nanosecond region were found in addition to the two longer-lived ones already known. Only one of the four isomers is at high excitation. The level scheme is complex and above about 6.7 MeV excitation, the decay strength is shared between several weak paths. Consequently it was not possible to assign spins to levels above that at 7502 keV (J = 24).

Semi-empirical shell-model calculations assuming a ^{208}Pb core and six valence particles give a satisfactory account of the energies of the observed odd-parity states and of the even-parity levels with J > 12. The energies of the even-parity levels with J = 6 to 12 agree better with those arising from the weak coupling of the configurations of two valence protons to a ^{204}Pb core in its 0^+_1, 2^+_1, and 4^+_1 states. At high excitation, while there is a suggestion that excited-core states may be present in the yrast sequence, the evidence is inconclusive. This is similar to the situation in the radon isotopes where such states have been

identified in [210, 211, 212]Rn [refs. [1, 2, 3] respectively] but not in [208, 209]Rn [refs. [23,33] respectively].

References

1) A. R. Poletti, G. D. Dracoulis, C. Fahlander and I. Morrison, Nucl. Phys. A380 (1982) 335

2) A. R. Poletti, G. D. Dracoulis, C. Fahlander and I. Morrison, Nucl. Phys. A359 (1981) 180;

    G. D. Dracoulis, C. Fahlander and A. R. Poletti, Phys. Rev. C24 (1981) 2386

3) D. Horn, O. Häusser, T. Faestermann, A. B. McDonald, T. K. Alexander, J. R. Beene and C. J. Herrlander, Nucl. Phys. A317 (1979) 520

4) A. P. Byrne, G. D. Dracoulis, C. Fahlander, H. Hübel, A. R. Poletti, A. E. Stuchbery, J. Gerl, R. F. Davie and S. J Poletti, Nucl. Phys. A448 (1986) 137;

    A. P. Byrne, R. Müsseler, H. Hübel, M. Murzel, K. Theine, W. Schmitz, K. H. Maier, H Kluge, H. Grawe and H. Haas, Phys. Lett. B217 (1989) 38

5) A. P. Byrne and G. D. Dracoulis, Nucl. Phys. A391 (1982) 1

6) T. Lönnroth, "Experimental and theoretical two-nucleon interaction energies in the lead region", Department of Physics, University of Jyväskylä internal report (1982) unpublished

7) I. Bergström, J. Blomqvist, C. J. Herrlander and K. Wikström, Phys. Scripta 10 (1974) 287

8) M. P. Webb, Nucl. Data Sheets 26 (1979) 145

9) V. Rahkonen, B. Fant and C. J. Herrlander, Phys. Scripta 34 (1986) 720

10) M. Ishii, Nucl. Instr. Meth. 127 (1975) 53

11) O. Dragoun, V. Brabec, A. Maštalka, A. Kovalík, M. Ryšavý, M. Ya. Kuznetsora and Yu. V. Norseev, Nucl. Phys. A391 (1982) 29

12) B. Fant, Phys. Scripta 4 (1971) 175

13) N. Bräuer, A. Goldmann, J. Hadijuana, M. von. Hartrott, K. Nishiyama, D. Quitmann, D. Riegel, W. Zeitz and H. Schweickert, Nucl. Phys. A206 (1973) 452

14) F. Rösel, H. M. Fries, K. Alder and H. C. Pauli, At. Nucl. Data Tables 21 (1978) 291

15) V. Rankonen, I. Bergström, J. Blomqvist, O Knuutilla, K. -G. Rensfelt, S. Szarkier and K. Westerberg, Z. Phys. A284 (1978) 357; V. Rahkonen, Ph.D. dissertation, University of Jyväskylä research report 10/1980, unpublished

16) A. H. Wapstra and G. Audi, Nucl. Phys. A432 (1985) 55

17) M. J. Martin, Nucl. Data Sheets 47 (1986) 797

18) T. T. S. Kuo and G. H. Herling, NRL Report 2258, Naval Research Laboratory, Washington (1971)

19) N. Roy, K. H. Maier, A. Aprahamian, J. A. Becker, D. J. Decman, E. A. Henry, L. G. Mann, R. A. Meyer, W. Stoeffl and G. L. Struble, Phys. Lett. B221 (1989) 6

20) T. Lönnroth, Z. Phys A307 (1982) 175

21) H. Hübel, M. Gottormsen, K. P. Blume, J. Recht, A. Von. Grumbkov, K. Hardt, P. Schüler, Y. K. Agarwal and A. Maj, Z. Phys A314 (1983) 89

22) J. Blomqvist, I. Bergström, C. J. Herrlander, C. G. Linden, and K. Wikström, Phys. Rev. Lett. 38 (1977) 534

23) W. J. Triggs, A. R. Poletti, G. D. Dracoulis, C. Fahlander and A. P. Byrne, Nucl. Phys. A395 (1983) 274

24) I. Bergström, J. Blomqvist, B. Fant, C. J. Herrlander, V. Rahkonen and K. Wikström, Annual report, Research Institute of Physics, Stockhom (1974) 3.3.33

25) C. G. Lindén, I. Bergström, J. Blomqvist, K.-G. Rensfelt, H. Sergolle and K. Westerberg, Z. Phys. A277 (1976) 273

26) M. P. Webb, Nucl. Data Sheets 26 (1979) 145

27) M. J. Martin, Nucl. Data Sheets 22 (1977) 545

28) O. Häusser, T. K. Alexander, J. R. Beene, E. D. Earle, A. B. McDonald, F. C. Khanna and I. S. Towner, Nucl. Phys. A273 (1976) 253

29)   V. Rahkonen and T. Lönnroth, Nucl. Phys. A464 (1967) 349

30)   R. G. Helmer and C. W. Reich, Phys. Rev. C27 (1983) 2248

31)   U. Rosengård, I. Bergström, J. Blomqvist, P. Carlé, A. Källberg, L. O. Norlin and K. -G. Rensfelt, Phys. Scripta 31 (1985) 122

32)   I. Bergström, J. Blomqvist, C. J. Herrlander, J. Hattula, O. Knuuttila, E. Liukkonen and V. Rahkonen, Z. Phys. A287 (1967) 219

33)   A. R. Poletti, G. D. Dracoulis, C. Fahlander and A. P. Byrne, Nucl. Phys. A440 (1985) 118

TABLE 1

Summary of experimental conditions

Experiment type	Detectors and angles [a]		Beam energy and pulsing	Target angle [b]
Excitation functions		CSS, +90°	70, 75, 78, 80 MeV	45°
		CSS, -120°	not pulsed	
$\gamma - \gamma$ coincidences	(i)	CSS, +90°	78 MeV	45°
		CSS, -120°	not pulsed	
	(ii)	HPGe, +135°	78 MeV	0°
		HPGe, -135°	not pulsed	
		LEPS, +45°		
		LEPS, -45°		
Timing relative to beam		HPGe, +45°	78 MeV	0°
		LEPS, -45°	1 ns pulses	
		NE213, 135°	1 μs apart	
Internal conversion		CSS, +55°	78 MeV	0°
		Si(Li), -125°	1 ns pulses	
			1 μs apart	
Angular distributions		HPGe, +45° → 155°	78 MeV	45°
		HPGe, -90°	not pulsed	

a)   CSS denotes Compton-suppressed spectrometer; HPGe denotes coaxial hyperpure germanium detector; LEPS denotes planar, germanium, low-energy photon spectrometer; NE213 denotes liquid scintillator for neutron detection; Si(Li) denotes lithium-drifted, silicon detector and mini-orange magnetic filter for electron detection. Detector angles are relative to the beam direction.

b)   Angle between the normal to the target and the beam direction.

TABLE 2

Properties and placements of γ-rays assigned to [206]Po

Energy [a] (keV)	Energy of emitting state (keV)	Relative intensity	A_2/A_0	A_4/A_0
(12.5) [b]	1585.6			
(18.3) [b]	3567.1			
33.7	4685.3	0.10(2)		
39.0	4651.2	0.09(2)		
43.1				
44.0	4612.9	0.08(2)	-	
61.8	2262.0	45(2)		
63.3	3548.8	0.7(5)		
85.6	6958.0	2(1)		
85.8	4568.8	0.8(4)		
86.0	3548.8	16.0(5)	-0.24(03)	-0.03(05)
115.5	6050.5	0.5(1)		
116.8	8381.3	0.2(1)		
119.5				
120.8	2901.4	0.6(1)	-0.33(13)	0.29(19)
136.8		0.9(1)	-0.29(09)	0.06(12)
138.9	1573.1	1.0(1)	-0.07(08)	-0.03(12)
146.2	4831.8	5.2(2)	-0.30(02)	-0.02(03)
163.4	8381.3	1.0(2)	-0.13(07)	-0.03(11)
165.6	5334.2	2.2(2)	-0.25(03)	-0.03(05)
167.9	2780.6	3.2(3)	-0.28(02)	0.01(04)
169.8	6288.0	5.1(5)	-0.29(02)	-0.07(03)
170.2	2432.1	0.8(2)		
179.5	5513.7	1.9(2)	-0.31(04)	0.01(06)
180.5	8381.3	0.7(2)		
183.2	6118.2	8.0(5)	-0.31(01)	-0.05(02)
189.8	2612.7	2.3(3)	-0.45(03)	0.01(05)
195.0		0.6(1)		
196.7		1.9(2)	-0.15(06)	-0.27(10)
200.3	7158.2	2.5(2)	-0.34(04)	-0.08(08)
203.3		1.1(2)		
212.4	8643.0	4.5(2)	-0.10(04)	-0.04(06)
215.0		1.6(2)	-0.23(07)	0.09(11)
224.1	2656.2	1.3(2)		
237.6	2565.2	18.6(4)	-0.23(01)	-0.02(02)
245.8	8627.1	2.2(2)	-0.35(05)	0.01(07)
252.5	3462.8	1.5(2)	-0.53(06)	-0.35(09)
256.4	1434.1	1.7(2)	-0.17(05)	-0.04(07)
267.7		1.4(2)		
270.6	8897.7	2.2(2)	-0.40(04)	-0.11(07)
292.9	6343.4	1.5(3)	-0.58(11)	-0.08(14)
300.6		1.0(5)		
317.6	5486.2	2.3(1)		
326.5		1.2(1)		

[a] Uncertainties range from 0.1 keV for strong lines to 0.3 keV for weak lines.
[b] Unobserved transitions inferred from γ-γ coincidence data and energy sums.

TABLE 2 (continued)

Properties and placements of γ-rays assigned to [206]Po

Energy [a] (keV)	Energy of emitting state (keV)	Relative intensity	A_2/A_0	A_4/A_0
336.5	7473.5	2.0(2)	-0.28(05)	-0.06(08)
343.8	7502.0	2.5(3)	-0.36(05)	0.12(08)
344.2		1.3(5)		
350.8	8993.8	7.1(3)	-0.21(05)	0.15(11)
362.1	2780.6	2.6(3)	-0.47(07)	-0.27(11)
380.6	5212.4	12.9(5)	-0.46(02)	-0.01(02)
384.0		0.8(2)		
395.0	3462.8	48(2)	-0.10(01)	-0.05(01)
395.5	1573.1	94(2)		
396.9	7593.2	0.3(2)		
402.4	7158.2	1.3(5)		
416.3		1.4(2)	-0.53(09)	-0.41(04)
421.8	7121.0	1.9(3)	-0.35(06)	0.07(09)
422.6		1.0(3)		
429.3	3209.9	3.8(4)	-0.42(04)	0.04(05)
440.6	7196.3	3.5(5)	-0.41(08)	0.32(19)
457.0	5168.6	8.5(5)	-0.40(02)	-0.01(03)
457.2		1.7(7)		
466.0	3951.5	4.7(5)	-0.26(03)	-0.10(05)
467.7	6755.7	7(1)	-0.43(02)	-0.02(03)
468.0	6477.5	2.7(5)		
469.6	4632.5	6.3(6)	-0.50(03)	-0.06(05)
477.0	1177.6	98.4(4)	0.01(01)	-0.03(01)
481.3	4711.6	1.1(2)		
495.8	6009.5	5.4(3)	-0.42(03)	0.07(04)
504.9	6982.4	1.4(3)	-0.59(09)	0.31(14)
510.5		1.7(2)		
522.5	4685.6	0.9(2)		
526.2	4230.3	1.1(2)	0.00(03)	0.02(05)
541.7	8043.7	0.5(1)		
544.5		3(1)		
557.7	5935.0	11.0(5)	-0.36(02)	0.04(03)
558.1				
561.1	3462.8	1.1(3)	-0.36(11)	-0.26(20)
568.2	7267.4	2(1)	0.10(07)	0.01(10)
581.0	6699.2	2.6(5)	-0.19(01)	-0.02(02)
581.1	4744.0	2.7(5)		
595.8	4162.9	17.1(5)	-0.47(01)	-0.00(02)
600.8	5935.0	4(1)	-0.21(04)	-0.15(06)
607.8	8430.6	0.6(1)		
614.6	2200.2	45(1)	0.01(01)	-0.05(01)
617.3	4568.8	2.4(5)	0.13(08)	0.05(13)
622.9	5334.2	1.7(7)		
626.4	7822.7	1.4(4)		
627.1	2200.2	1.5(4)	-0.24(12)	-0.26(17)
633.3	5377.3	1.8(2)	-0.04(07)	0.20(12)
647.4	6521.6	1.8(2)	-0.52(06)	0.33(09)

[a] Uncertainties range from 0.1 keV for strong lines to 0.3 keV for weak lines

TABLE 2 (continued)

Properties and placements of γ-rays assigned to [206]Po

Energy [a) (keV)	Energy of emitting state (keV)	Relative intensity	A_2/A_0	A_4/A_0
661.3	4612.9	2.5(5)	-0.34(02)	0.05(03)
661.8	5874.2	3.5(5)		
670.0	6958.0	4(1)	-0.29(10)	-0.15(10)
676.4	2262.0	7.9(5)	-0.03(02)	0.02(04)
679.7	6699.2	0.6(1)		
682.0	5513.7	4(1)	-0.56(04)	0.07(06)
700.6	700.6	100	0.01(01)	-0.05(01)
722.4	5935.0	5(1)	0.30(01)	-0.04(02)
730.5	9724.3	1.2(3)	-0.09(09)	0.03(14)
733.5	1434.1	1.0(1)	0.03(10)	-0.13(17)
744.8	5377.3	7.2(5)	-0.48(02)	0.10(04)
754.5	6872.7	2.2(4)	-0.49(07)	0.01(11)
759.9	7281.5	2.6(3)	-0.05(06)	0.19(07)
793.6	7137.0	2.0(5)	-0.32(06)	0.11(10)
793.8		1.0(5)		
805.9	3067.9	46(5)	0.21(01)	-0.06(01)
806.6	3462.8	11(2)		
807.1	6019.5	0.6(3)		
829.3	3485.5	7.0(5)	0.35(10)	-0.02(10)
833.0	2418.6	26(2)	0.20(05)	-0.08(05)
837.2	2422.8	9(2)	-0.39(01)	0.05(02)
837.2	8430.6	0.3(2)		
901.8	3558.0	2(1)	-0.99(12)	0.18(16)
919.2	8200.8	1.4(2)	-0.54(08)	0.16(12)
928.6	8430.6	1.0(3)		
936.2	4494.2	2(1)	-0.43(05)	0.01(07)
936.2	8348.4	1.0(2)		
957.3	8430.6	0.7(2)	-0.54(15)	-0.33(20)
977.2	8258.7	0.9(2)		
979.2	7267.4	0.8(1)		
983.2	8264.6	0.7(1)	-0.77(14)	-0.07(24)
1027.3	2612.7	4.9(4)	0.15(03)	-0.10(04)
1045.9	4612.9	0.9(2)		
1047.9	3704.1	3.0(3)		
1064.1	4612.9	6.1(5)	-0.29(03)	-0.01(07)
1065.8	4632.5	3.2(4)	0.33(07)	0.11(12)
1084.8	4651.9	2.3(3)		
1103.3	5935.0	2.5(3)	-0.21(04)	0.02(06)
1124.2	7412.2	1.4(2)		
1125.3				
1131.0				
1144.5	4711.6	7.6(5)	-0.32(02)	0.04(03)
1191.2	5935.0	0.8(2)	0.35(21)	-0.42(28)
1214.3	5377.3	0.6(2)	0.11(17)	0.13(26)
1235.7	8218.0	0.7(2)	-0.11(13)	0.00(22)
1273.1	4483.1	1.6(2)	-0.59(06)	-0.12(10)
1285.6	3704.1	1.1(3)		
1293.2		1.2(2)		

a) Uncertainties range from 0.1 keV for strong lines to 0.3 keV for weak lines

TABLE 2 (continued)

Properties and placements of γ-rays assigned to [206]Po

Energy [a]) (keV)	Energy of emitting state (keV)	Relative intensity	A_2/A_0	A_4/A_0
1302.7	5935.0	0.8(2)	-0.09(10)	-0.11(15)
1311.5		1.1(2)		
1358.9	4568.8	1.9(2)	0.17(05)	0.03(08)
1581.8	4483.1	1.0(1)		
1667.2	4568.8	1.3(1)	0.28(07)	0.02(11)
1702.9	4483.1	1.0(1)	0.18(09)	-0.14(14)

[a]) Uncertainties range from 0.1 keV for strong lines to 0.3 keV for weak lines

TABLE 3

Mean lives of [206]Po levels

Level energy (keV)	Mean life (nsec)		
	Present work	Rahkonen et al. [9]	Broda et al. [a]
1585.6	335(6)	303(14)	310(7)
2262.0	1520(90)	1440(290)	
2656.2	0.7(2)	<1	
8643.0	1.5(4)		

[a] Quoted in refs. [8,9]

TABLE 4

Assignments from internal conversion measurements

		Internal conversion coefficients (x100)						
		Experiment		Theory [a]				Deduced multipolarit
E_γ (keV)	Type [b]		E1	E2	E3	M1	M2	
33.7	T	5000(800)	186	$>10^5$	$>10^7$	5500	$>10^5$	M1
39.0	T	4900(700)	125	65000	$>10^6$	3500	$>10^5$	M1
44.0	T	3700(600)	91	36000	$>10^6$	2500	$>10^5$	M1
61.8	T	6.6(26)	36	7000	$>10^5$	910	29000	E1
86.0	T	300(30)	14.8	1450	40000	350	6900	M1
120.8	T	600(110)	29	330	6700	690	4700	M1
138.9	T	240(60)	20	188	3100	460	2800	E2
146.2	T	350(30)	17.9	154	2400	400	2300	M1
165.6	T	200(50)	13.2	95	1240	280	1490	M1(E2)
167.9	T	260(50)	12.7	90	1150	270	1420	M1
169.8	T	290(50)	12.4	87	1090	260	1360	M1
179.5	T	280(40)	10.8	71	820	220	1120	M1
183.2	T	240(30)	10.3	65	740	210	1040	M1
189.8	T	290(100)	9.4	58	620	191	920	M1
237.6	T	21(11)	5.4	26	210	102	420	E1
	L	<2.8	0.79	11.2	129	14.4	86	
	M	<1.4	0.29	2.9	36	3.4	22	
252.5	T	<30	4.7	22	157	86	340	E1,E2
344	K	65(8)	1.90	5.0	13.1	30	93	(M1)
362	K	28(6)	1.69	4.4	11.6	26	79	M1
381	K	27(1)	1.51	4.0	10.4	23	68	M1
	L	4.0(5)	0.26	1.87	13.3	4.0	16.1	
395 [c]	K	3.81(14)	1.40	3.7	9.5	21	61	E2
	L	1.65(10)	0.24	1.65	11.3	3.6	14.2	
	M	0.76(4)	0.05	0.42	3.0	0.85	3.5	
395	K	4.13(14)	1.40	3.7	9.5	21	61	E2
	L	1.65(11)	0.24	1.65	11.3	3.6	14.2	
429	K	17.5(13)	1.17	3.1	7.9	16.6	47	M1
	L	7.2(11)	0.20	1.25	7.9	2.9	10.8	
457	K	17.6(9)	1.02	2.7	6.8	14.0	39	M1
468	K	16(4)	0.98	2.6	6.5	13.3	36	M1
	L	4.1(7)	0.16	0.94	5.5	2.3	8.2	
470	K	19(4)	0.97	2.5	6.4	13.0	36	M1
	L	4.9(9)	0.16	0.92	5.3	2.2	8.0	
477 [c]	K	3.2(2)	0.94	2.5	6.2	12.5	34	E2
	L	1.01(6)	0.16	0.88	5.0	2.2	7.6	
	M	0.27(2)	0.04	0.22	1.33	0.51	1.87	
558	K	8.3(5)	0.68	1.79	4.4	8.3	22	M1
	L	<3.9	0.11	0.53	2.7	1.42	4.6	

TABLE 4 (continued)

		Internal conversion coefficients (x100)						
		Experiment	Theory [a]					Deduced multipolarity
E_γ (keV)	Type [b]		E1	E2	E3	M1	M2	
581	K	7.1(6)	0.63	1.65	4.0	7.5	19.1	M1
	L	1.1(3)	0.10	0.47	2.3	1.27	4.1	
596	K	7(4)	0.60	1.57	3.8	7.0	17.8	M1
	L	2.5(13)	0.10	0.44	2.1	1.19	3.7	
615 [c]	K	5.8(2)	0.57	1.48	3.5	6.5	16.3	M1
	L	1.05(4)	0.09	0.40	1.84	1.10	3.4	
	M	0.21(1)	0.02	0.10	0.48	0.26	0.83	
676 [c]	K	1.5(1)	0.47	1.22	2.9	5.0	12.4	(E2) [d]
	L	0.18(5)	0.08	0.32	1.30	0.85	2.5	(E1)
701 [c]	K	1.22(5)	0.44	1.14	2.7	4.6	11.2	E2
	L	0.27(1)	0.07	0.29	1.15	0.78	2.3	
	M	0.08(1)	0.02	0.07	0.29	0.18	0.55	
745	K	2.8(2)	0.39	1.02	2.3	3.9	9.4	M1
	L	0.91(6)	0.06	0.27	0.92	0.66	1.89	
806	K	0.98(5)	0.34	0.88	1.98	3.2	7.6	E2
	L	0.28(2)	0.05	0.24	0.71	0.54	1.50	
829	K	<5.4	0.32	0.83	1.87	3.0	7.0	not M2
833	K	1.31(9)	0.32	0.82	1.85	2.9	6.9	E2(M1)
	L	0.37(6)	0.05	0.23	0.64	0.49	1.36	
837	K	2.3(2)	0.32	0.82	1.83	2.9	6.8	E3,M1
1027	K	0.4(2)	0.22	0.56	1.20	1.71	3.9	E1,E2
1064	K	0.25(4)	0.21	0.52	1.12	1.56	3.6	E1
1103	K	<0.4	0.19	0.49	1.04	1.42	3.2	E1(E2)
1145	K	0.15(2)	0.18	0.46	0.97	1.30	3.0	E1
1191	K	0.32(12)	0.17	0.43	0.89	1.17	2.7	E2(E1)

[a] Values from ref. [14]).

[b] T denotes total conversion coefficient with experimental values from intensity balance;

K, L, M denote K-, L-, M-shell conversion coefficients respectively.

[c] Experimental conversion coefficients from spectra delayed relative to beam pulses.

[d] Other data indicate that the K-shell conversion line is contaminated; see text.

TABLE 5

Configurations considered in the shell-model calculations

Even Parity			Odd Parity		
Protons	Neutrons	E_0 (keV) [a]	Protons	Neutrons	E_0 (keV) [a]
$h_{9/2}^2$	$p_{1/2}^{-2}f_{5/2}^{-2}$	1740	$h_{9/2}^2$	$p_{1/2}^{-2}f_{5/2}^{-1}i_{13/2}^{-1}$	2803
$h_{9/2}^2$	$p_{1/2}^{-2}i_{13/2}^{-2}$	3866	$h_{9/2}^2$	$p_{1/2}^{-1}f_{5/2}^{-2}i_{13/2}^{-1}$	3373
$h_{9/2}^2$	$f_{5/2}^{-2}i_{13/2}^{-2}$	5006	$h_{9/2}^2$	$p_{1/2}^{-1}f_{5/2}^{-1}p_{3/2}^{-1}i_{13/2}^{-1}$	3700
$h_{9/2}f_{7/2}$	$p_{1/2}^{-2}f_{5/2}^{-2}$	2637	$h_{9/2}^2$	$f_{5/2}^{-2}p_{3/2}^{-1}i_{13/2}^{-1}$	4270
$h_{9/2}i_{13/2}$	$p_{1/2}^{-2}f_{5/2}^{-1}i_{13/2}^{-1}$	4412	$h_{9/2}^2$	$p_{1/2}^{-1}i_{13/2}^{-3}$	5499
$h_{9/2}i_{13/2}$	$p_{1/2}^{-1}f_{5/2}^{-2}i_{13/2}^{-1}$	4982	$h_{9/2}i_{13/2}$	$p_{1/2}^{-2}f_{5/2}^{-2}$	3340
$h_{9/2}i_{13/2}$	$f_{5/2}^{-2}p_{3/2}^{-1}i_{13/2}^{-1}$	5879	$h_{9/2}i_{13/2}$	$p_{1/2}^{-2}i_{13/2}^{-2}$	5474
$h_{9/2}i_{13/2}$	$f_{5/2}^{-1}i_{13/2}^{-3}$	7678	$h_{9/2}i_{13/2}$	$f_{5/2}^{-2}i_{13/2}^{-2}$	6615

[a] See text for definition of E_0

TABLE 6

Single particle energies relative to a ^{204}Pb core

--

Configuration	J^π	Excitation energy in ^{205}Bi (keV) [a]
$\pi(h_{9/2}) \otimes {}^{204}\text{Pb}\,(0^+{}_1)$	$9/2^-$	0
$\pi(f_{7/2}) \otimes {}^{204}\text{Pb}\,(0^+{}_1)$	$7/2^-$	1001
$\pi(i_{13/2}) \otimes {}^{204}\text{Pb}\,(0^+{}_1)$	$13/2^+$	1592
$\pi(h_{9/2}) \otimes {}^{204}\text{Pb}\,(2^+{}_1)$	$13/2^-$	881
$\pi(h_{9/2}) \otimes {}^{204}\text{Pb}\,(2^+{}_1)$	$11/2^-$	796
$\pi(h_{9/2}) \otimes {}^{204}\text{Pb}\,(2^+{}_1)$	$9/2^-$	1044
$\pi(h_{9/2}) \otimes {}^{204}\text{Pb}\,(2^+{}_1)$	$7/2^-$	850
$\pi(h_{9/2}) \otimes {}^{204}\text{Pb}\,(4^+{}_1)$	$17/2^-$	1344
$\pi(h_{9/2}) \otimes {}^{204}\text{Pb}\,(4^+{}_1)$	$15/2^-$	1168
$\pi(h_{9/2}) \otimes {}^{204}\text{Pb}\,(4^+{}_1)$	$13/2^-$	1110
$\pi(h_{9/2}) \otimes {}^{204}\text{Pb}\,(4^+{}_1)$	$11/2^-$	1194

[a] Energies and assignments from refs. [20,21]

TABLE 7

Reduced transition probabilities in ^{206}Po

Transition	E_γ (keV)	Branching ratio (%) [a]	Mean Life (ns) [a]	α_T [b]	B(EL)↓ [c] e^2fm^{2L}	W.u.
$8^+_1 \rightarrow 6^+_1$	12.5	100	335(6)	4.60×10^4	170(3)	2.35(4)
$9^-_1 \rightarrow 8^+_1$	676.4	15(1)	1520(90)	0.006	$1.51(15) \times 10^{-10}$	$6.7(7) \times 10^{-11}$
$9^-_1 \rightarrow 8^+_2$	61.8	85(1)	1520(90)	0.37	$1.13(7) \times 10^{-6}$	$5.0(3) \times 10^{-7}$
$11^-_1 \rightarrow 10^+_1$	237.6	93(1)	0.7(2)	0.056	$5.6(17) \times 10^{-5}$	$2.5(8) \times 10^{-5}$

[a] Data from present work

[b] The theoretical total internal-conversion coefficients α_T are from Rösel et al. [14]. They are for the pure lowest-order multipole allowed by the spins and parities.

[c] The reduced transition rates B(EL) were calculated assuming that the $8^+ \rightarrow 6^+$ transition is pure E2 and the others are pure E1. Single particle estimates (the Weisskopf units) were calculated using the relation

$$B_W(EL) \downarrow = \frac{1}{4\pi} \left(\frac{3}{3+L} \right)^2 \left(1.2A^{1/3} \right)^{2L} e^2fm^{2L}$$

Figure Captions

Figure 1: Level scheme for [206]Po. The excitation energies and transition
energies are in keV and the widths of the arrows indicate the relative
intensities of the γ-rays. Unobserved low-energy transitions inferred
from the coincidence data are shown as dashed arrows. The symbol τ
on the right-hand side indicates that the adjacent level is an isomer;
the measured mean lives are given in table 3.

Figure 2: Spectra from the γ-γ coincidence data obtained with the
Compton-suppressed spectrometers. In the upper panel is the sum of
spectra of γ-rays preceding the 701, 477 and 395 keV γ-rays by 190 to
2520 ns. The lower panel shows the spectrum of γ-rays which
preceded the 615 keV γ-rays by 190 to 2520 nsec minus the spectrum of
those delayed relative to the 615 keV γ-rays by the same time interval.

Figure 3: Spectra obtained with the Compton-suppressed spectrometers of γ-rays
in prompt coincidence (± 140 ns) with the 596, 1144 and 146 keV
transitions.

Figure 4: Relative excitation functions, normalized to unity at 70 MeV, of some
of the more prominent [206]Po γ-rays.

Figure 5: Spectra from the γ-γ coincidence data obtained with the HPGe and
LEPS detectors (see table 1). In the upper panel is part of the LEPS
spectrum in prompt coincidence with 381 keV γ-rays in the HPGe
detectors. The lower panel shows the HPGe detector spectrum in
prompt coincidence with 39 keV γ-rays in the LEPS detectors.

Figure 6: Spectra obtained with the Compton-suppressed spectrometer of γ-rays
in prompt coincidence (± 140 ns) with the 183 and 212 keV transitions.

Figure 7: Time spectra from the γ-γ coincidence data.

Figure 8: The time spectrum of 238 keV γ-rays, detected in the LEPS, relative to the beam pulses. The upper panel shows a fit to the spectrum of a convolution of the prompt response function (PRF, see text) with the decay curve resulting from the 0.7 ns mean life deduced for the 2656.2 keV level.The lower panel shows the same spectrum and the PRF only. ¯

Figure 9: Spectra of internal conversion electrons in a Si(Li) detector and of the corresponding γ-rays detected with a Compton-suppressed spectrometer. The upper pair of spectra are of electrons and γ-rays detected within the range +20 to -40 ns relative to the 1 ns-wide beam pulses and the lower pair are of those delayed by 40 to 900 ns relative to the beam pulses.

Figure 10: Comparison of the even-parity states of ^{206}Po, observed in the present work, with those calculated with the empirical shell model. Each set of shell model states is labelled by its configuration. These labels are abbreviated but may be identified unambiguously with the configurations listed in table 5. Configuration labels marked with a dagger (†) are those in which the calculations involved more than two two-nucleon interaction energies not derived from experimental data. States marked with an asterisk (*) are those which, according to the calculations, would be yrast.

Figure 11: Comparison of the odd-parity levels of ^{206}Po, observed in the present work, with states calculated with the empirical shell model. For other details see the caption to figure 10.

Figure 12: Comparison of the energies of some of the lower-lying ^{206}Po states observed in the present work with those of states calculated with the shell model in which ^{206}Po is regarded as either two valence protons coupled to a ^{204}Po core in its 0^+_1, 2^+_1, and 4^+_1 states or as four neutron holes coupled to a ^{210}Po core. Likely identifications are indicated by dashed lines.
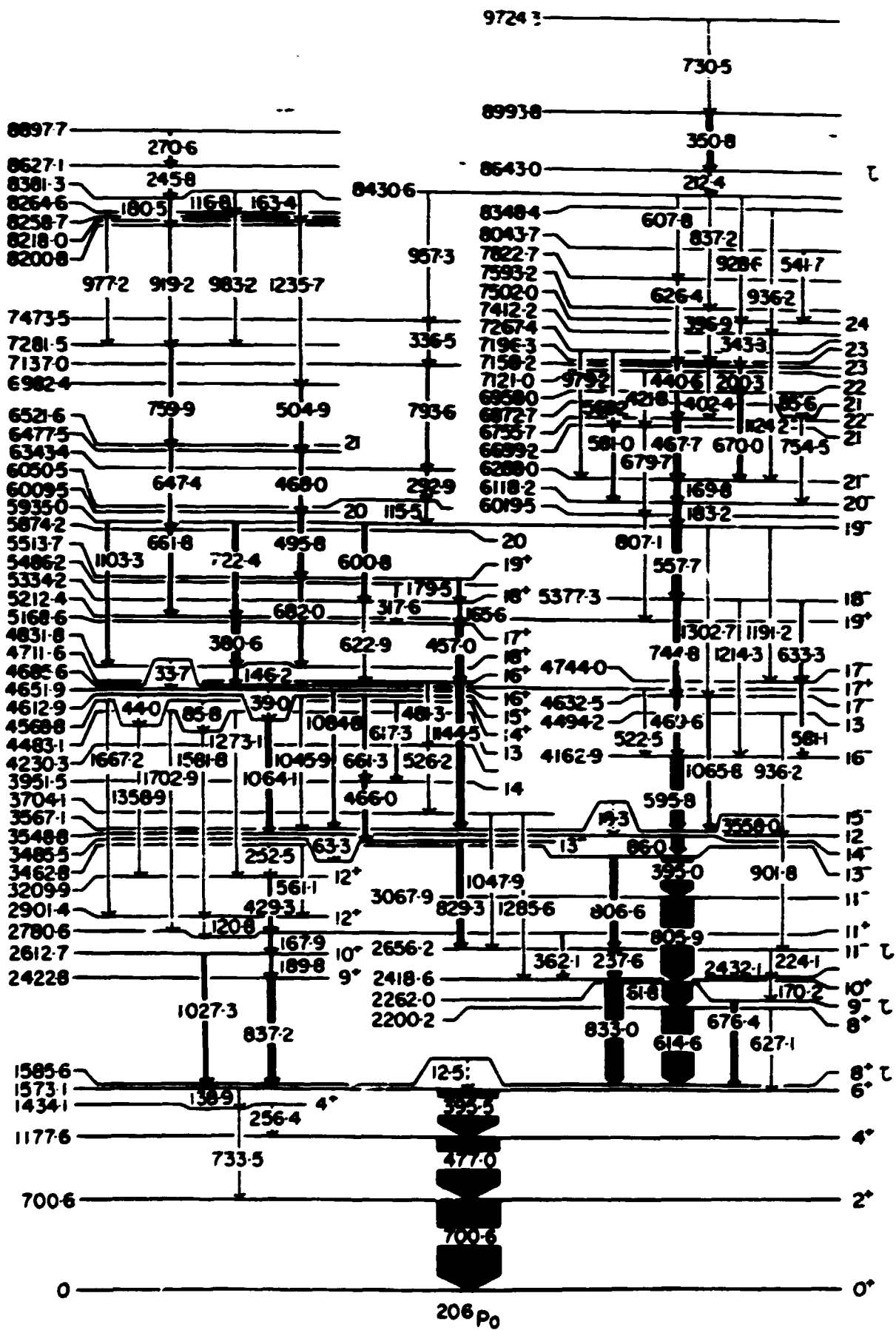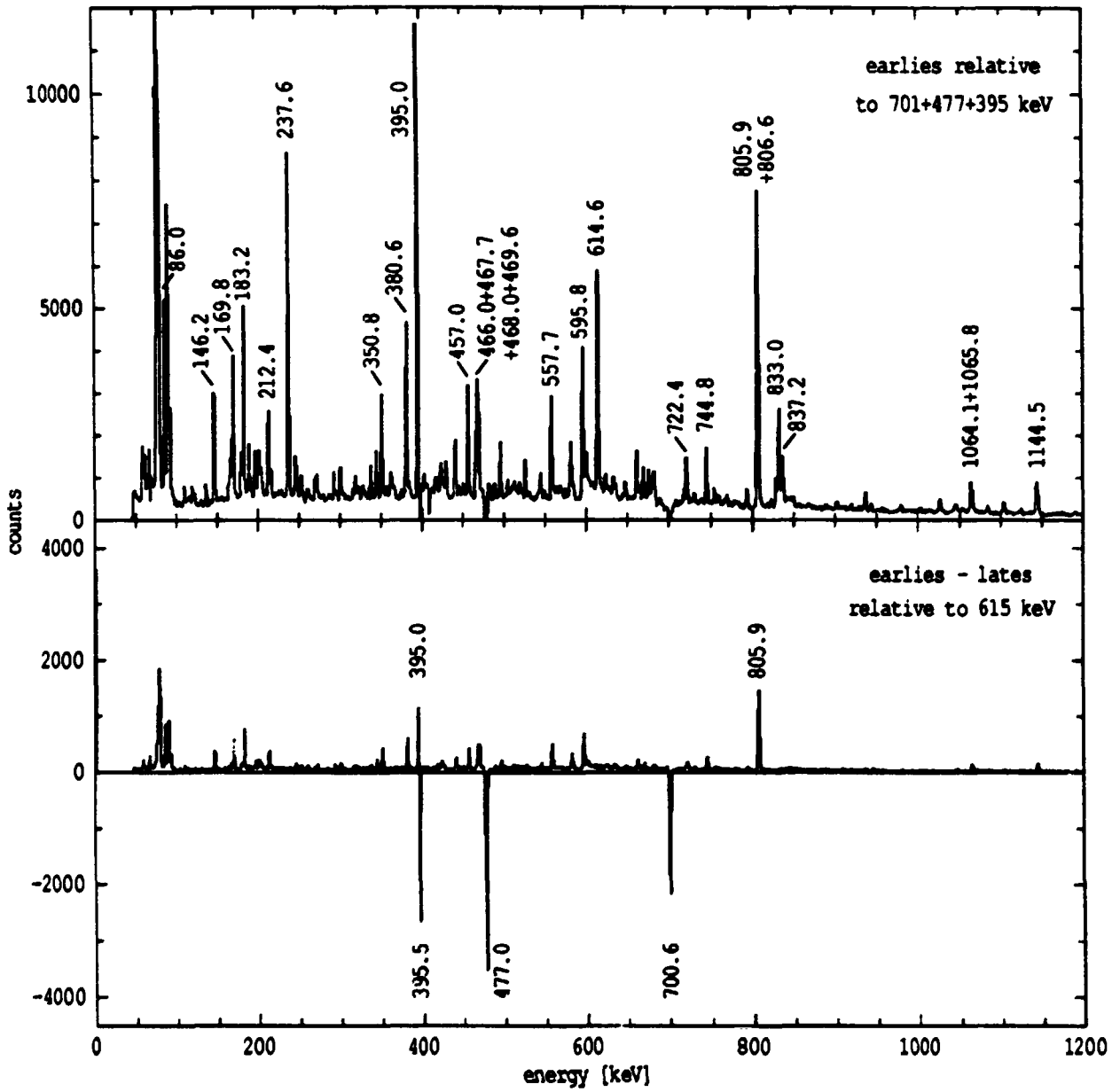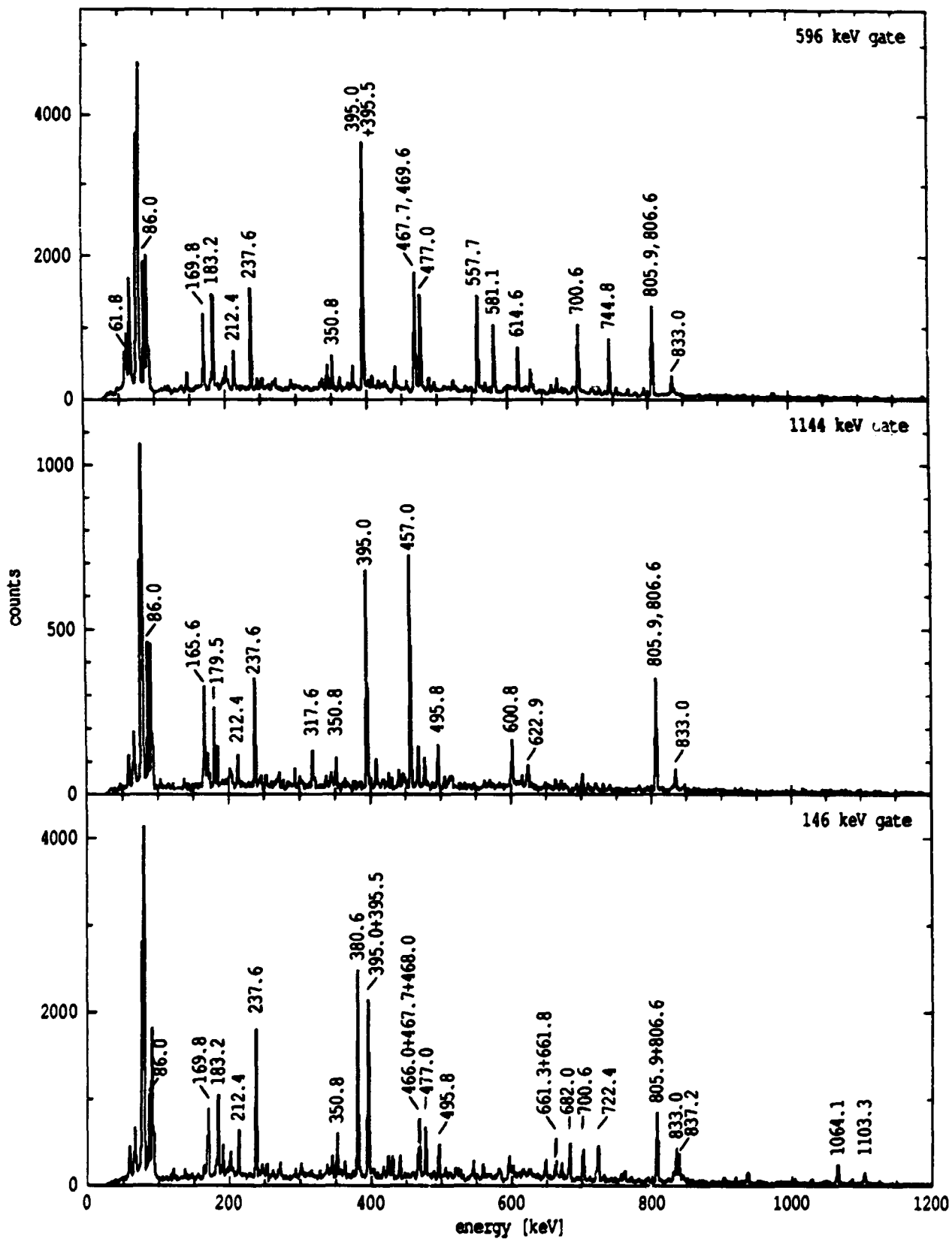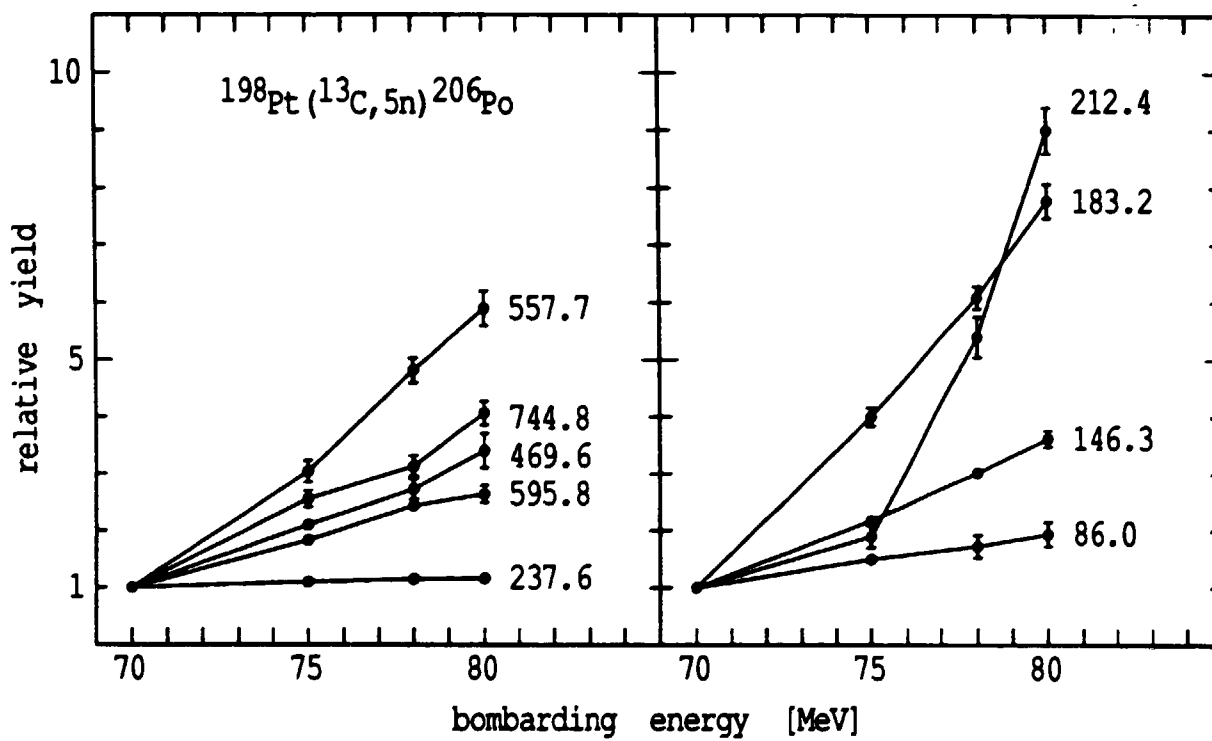
Figure 1

Figure 2

Figure 3

Figure 4

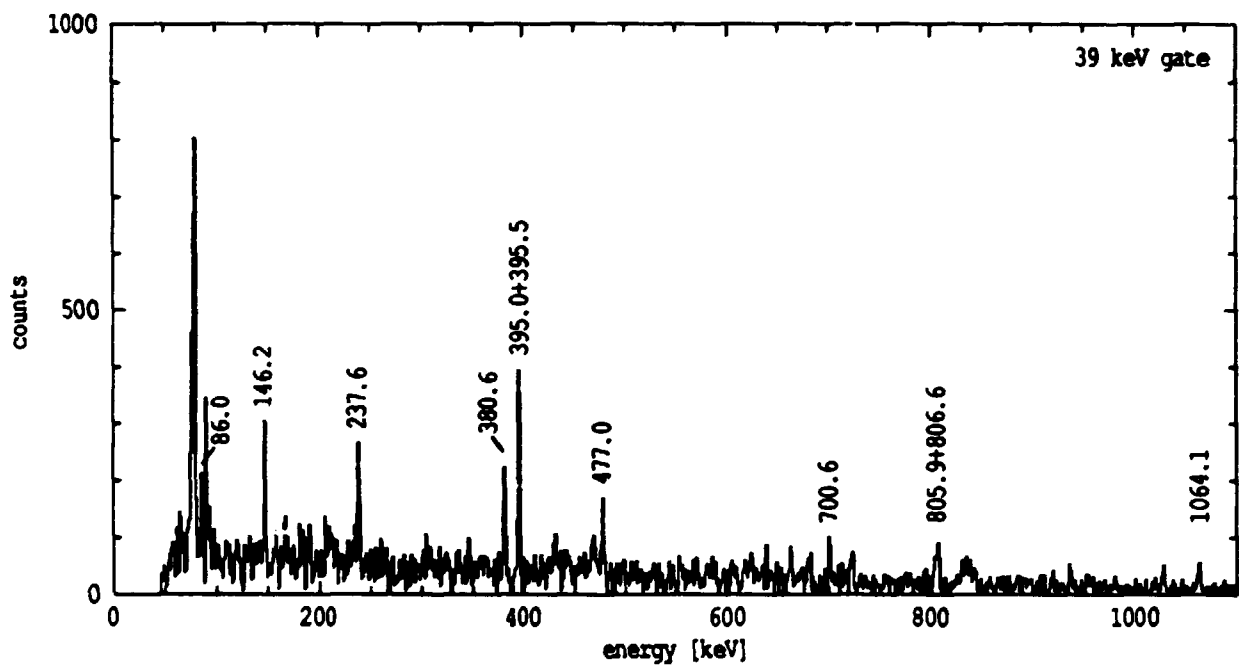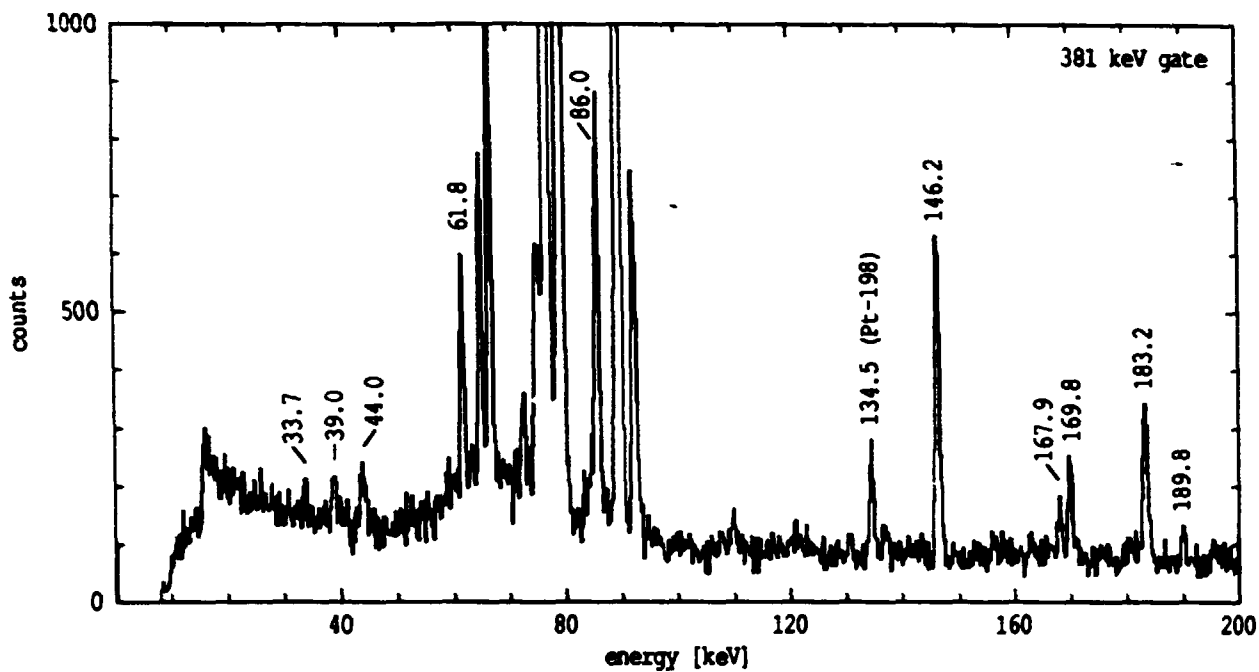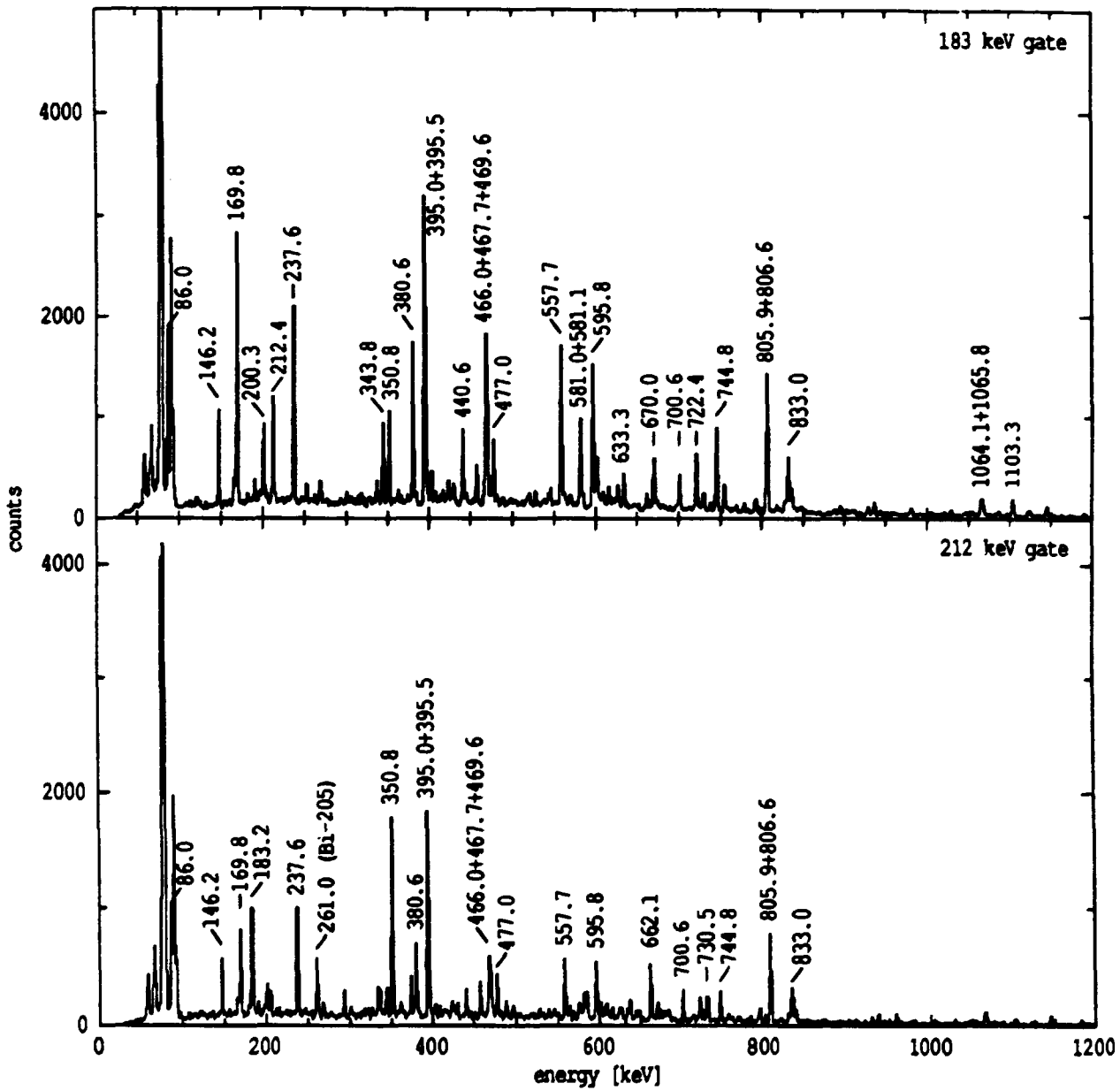Figure 5

Figure 6

477.0 keV
relative to 614.6 keV

395.0 + 395.5 keV
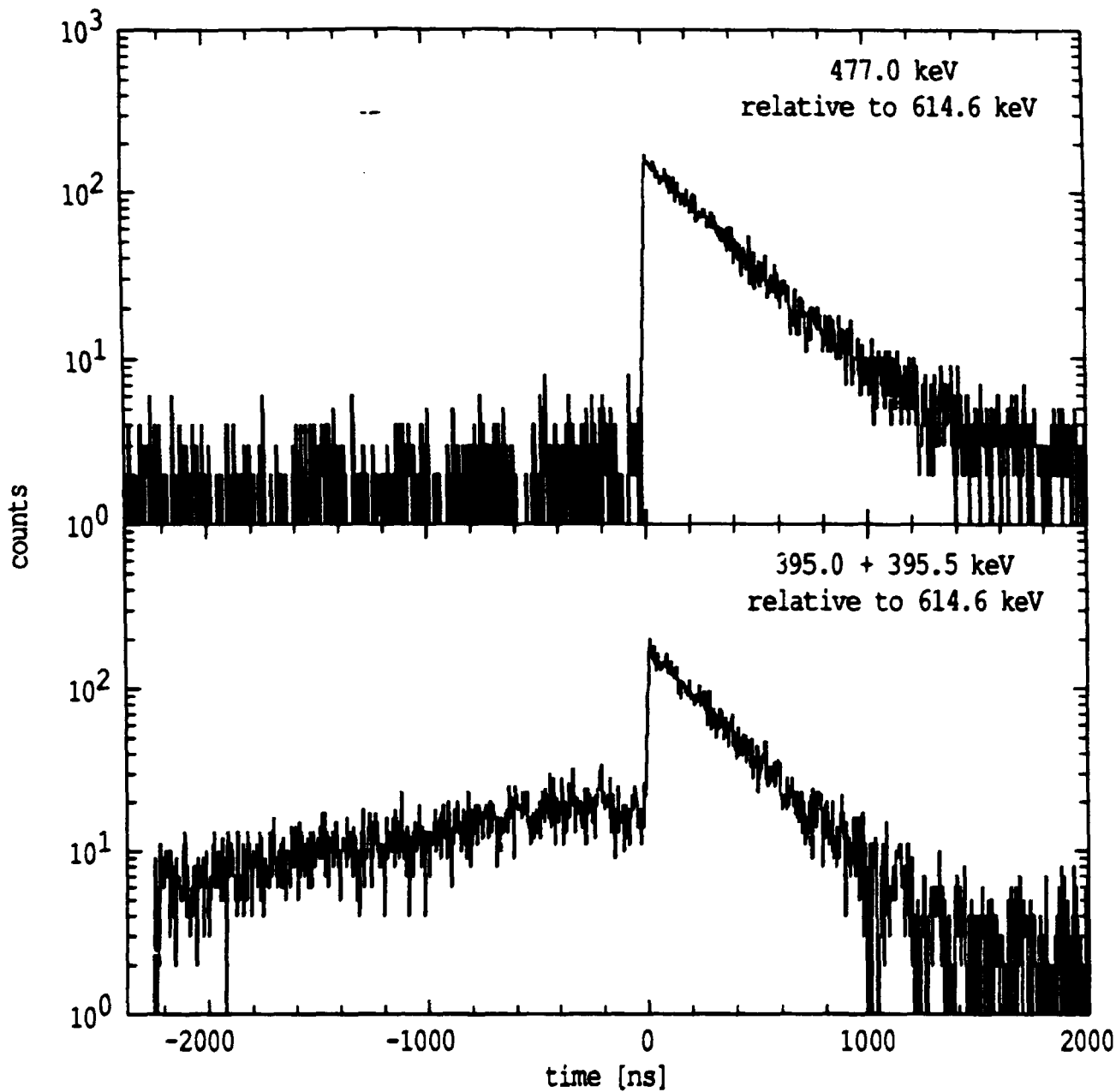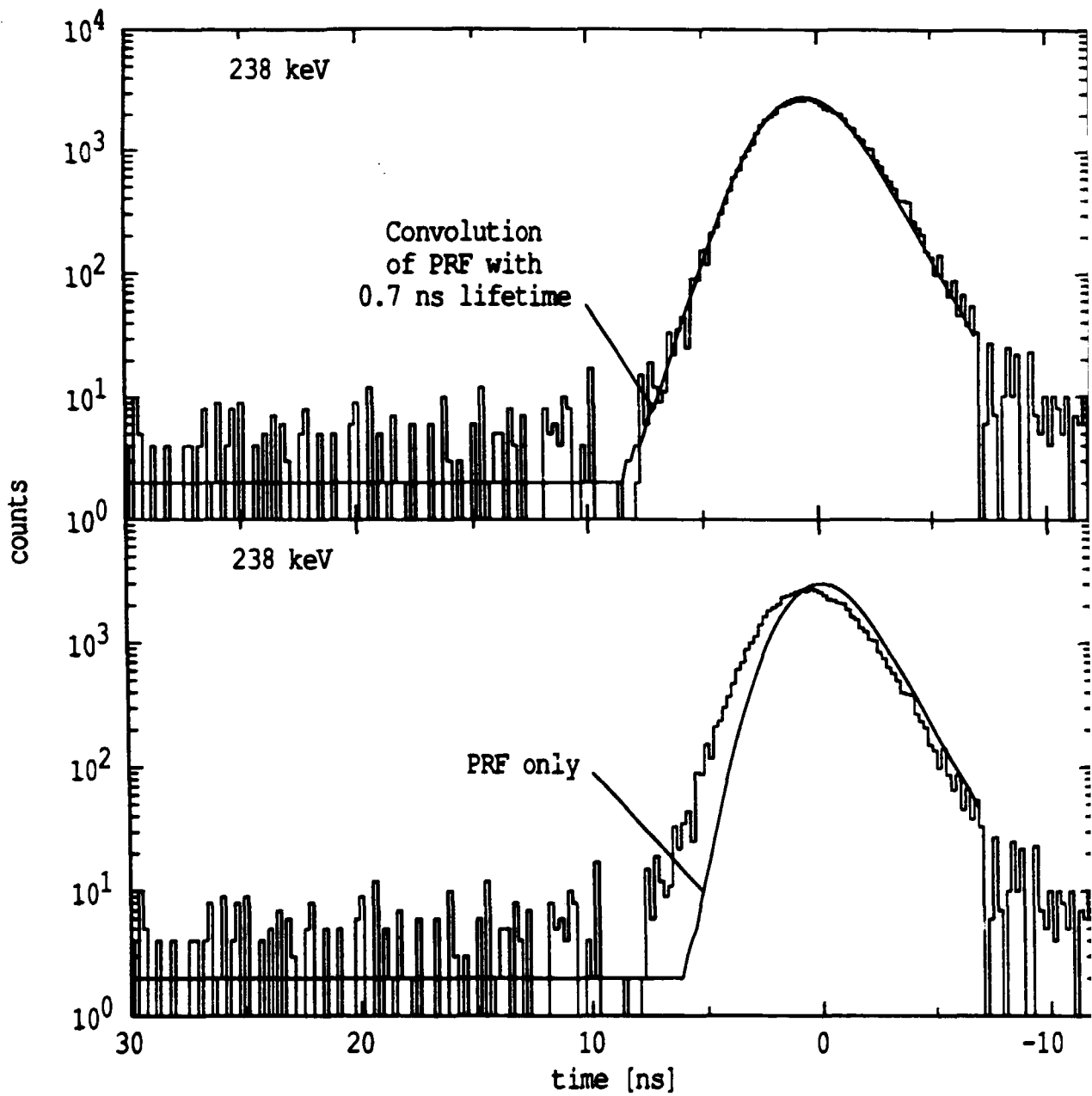relative to 614.6 keV
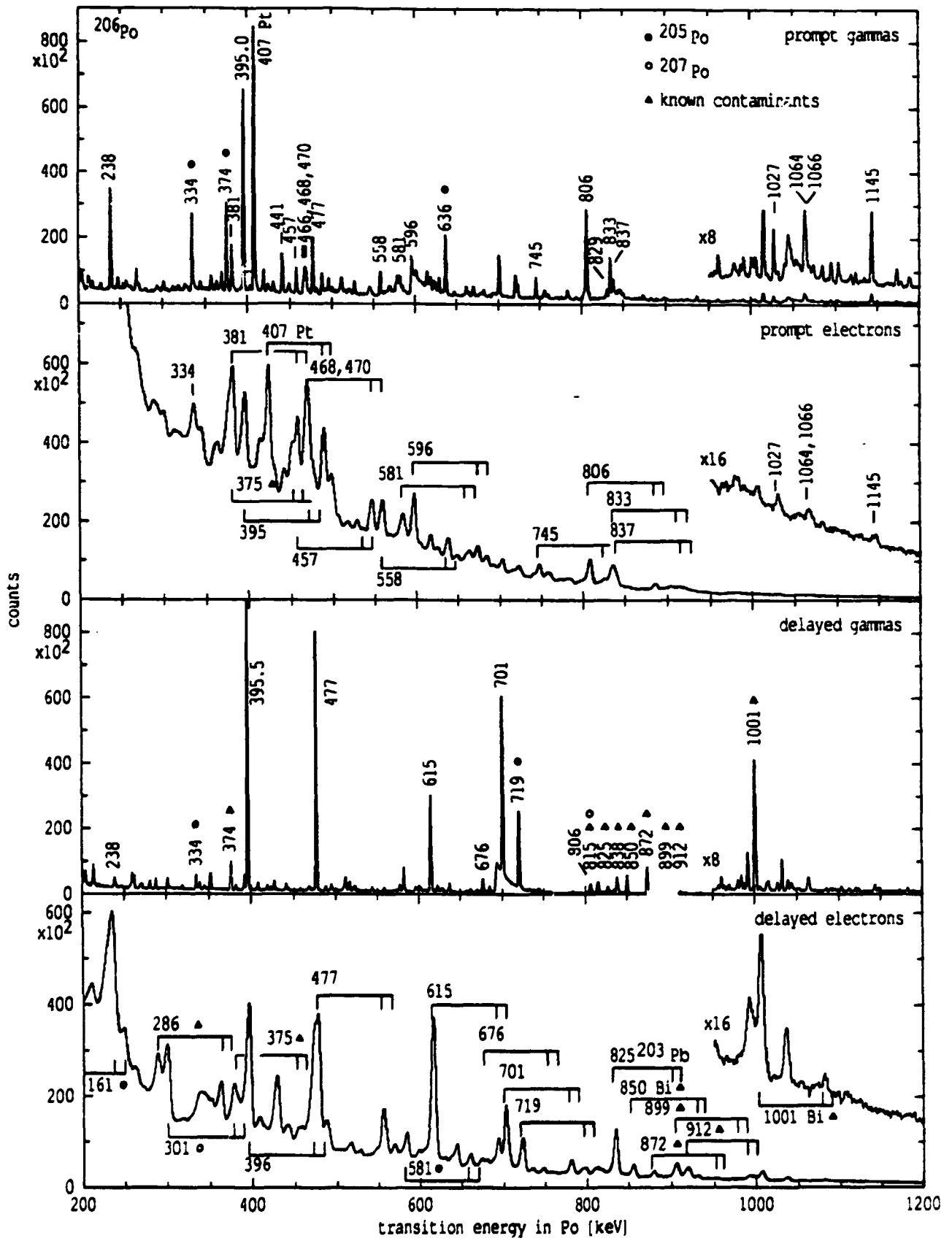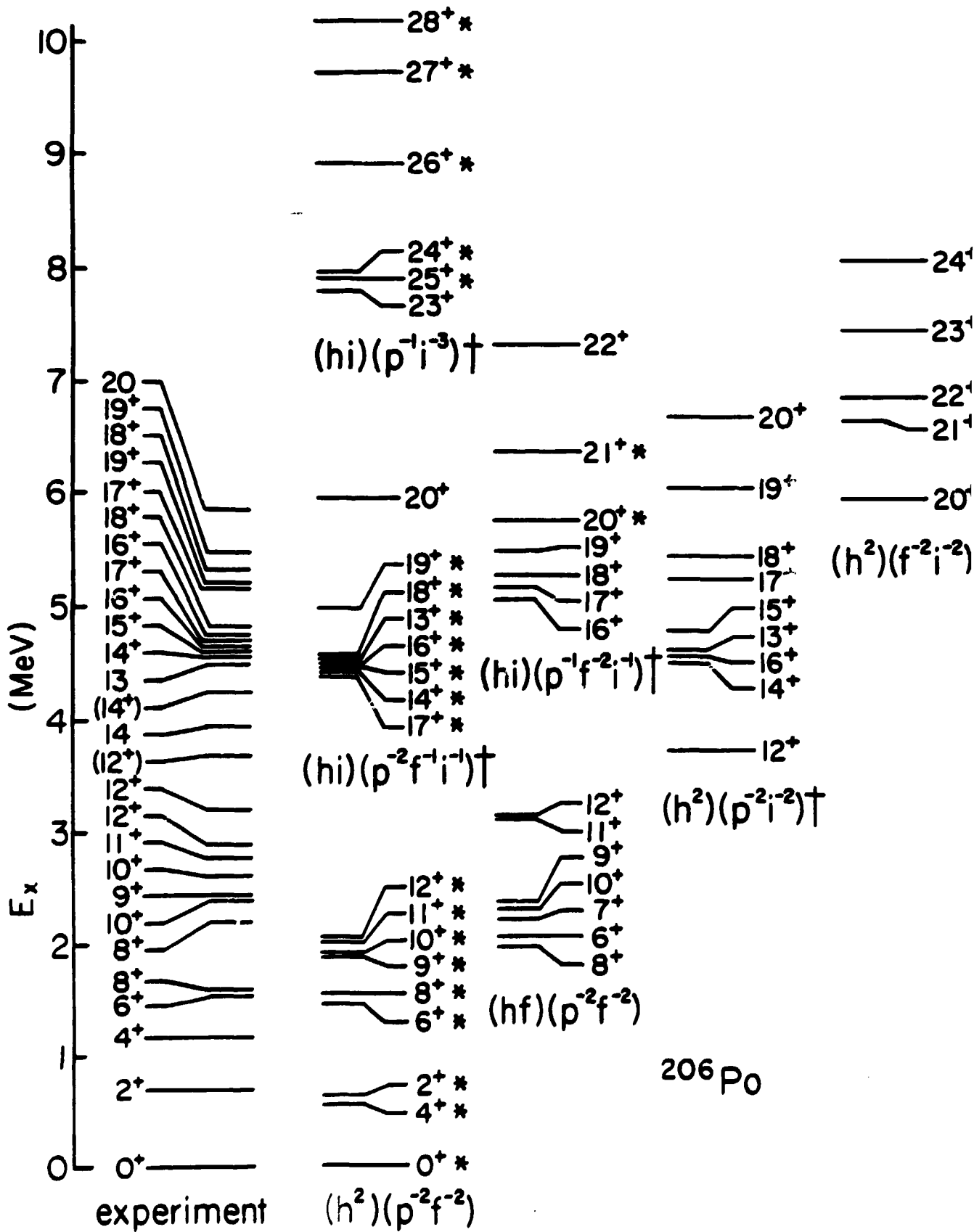
Figure 7

238 keV

Convolution
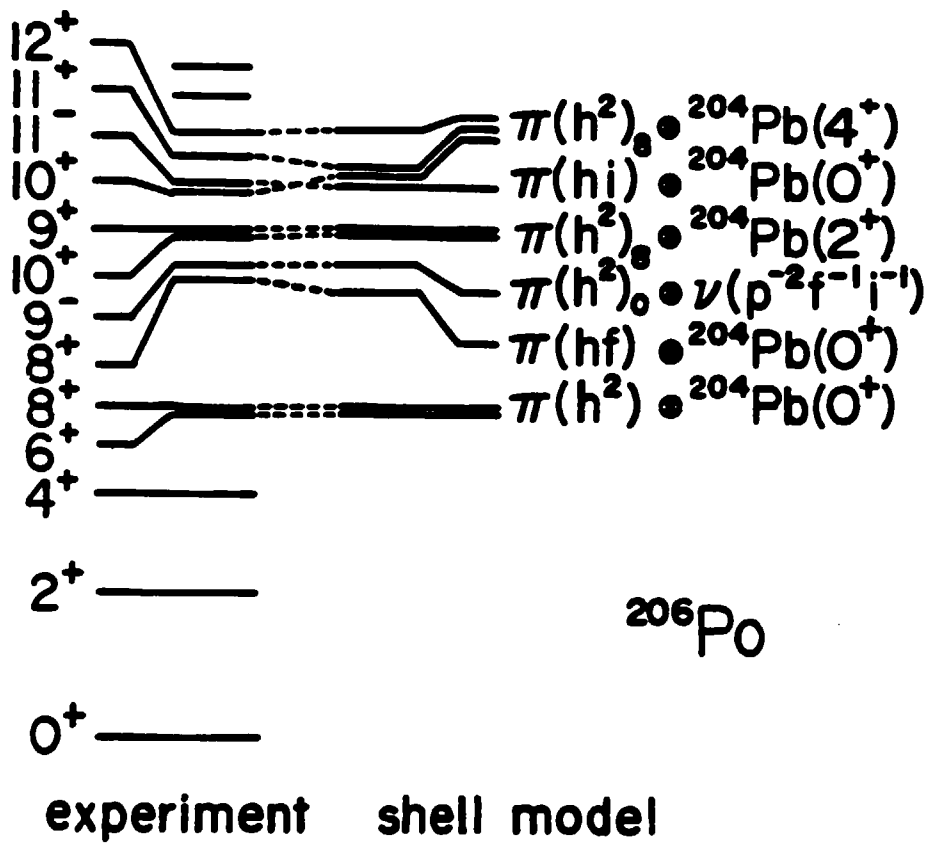of PRF with
0.7 ns lifetime

238 keV

PRF only

Figure 8

Figure 9

Figure 13

Figure 12

^{206}Po

$(h^2)(p^{-1}i^{-3})†$

$(hi)(f^{-2}i^{-2})†$

$(hi)(p^{-2}i^{-2})†$

$(h^2)(p^{-1}f^{-1}p^{-1}_{3/2}i^{-1})$

$(h^2)(f^{-2}p^{-1}_{3/2}i^{-1})$

$(h^2)(p^{-1}f^{-2}i^{-1})$

$(hi)(p^{-2}f^{-2})†$

$(h^2)(p^{-2}f^{-1}i^{-1})$

experiment

Figure 12